LA-UR-97-116

Title: MATERIALS CORROSION AND MITIGATION STRATEGIES FOR APT: END OF YEAR REPORT FOR FY96

Author(s): R. SCOTT LILLARD, MST-6
DARRYL P. BUTT, MST-6

Submitted to: END OF FY96 REPORT OF APT PROGRAM

DISCLAIMER

MASTER

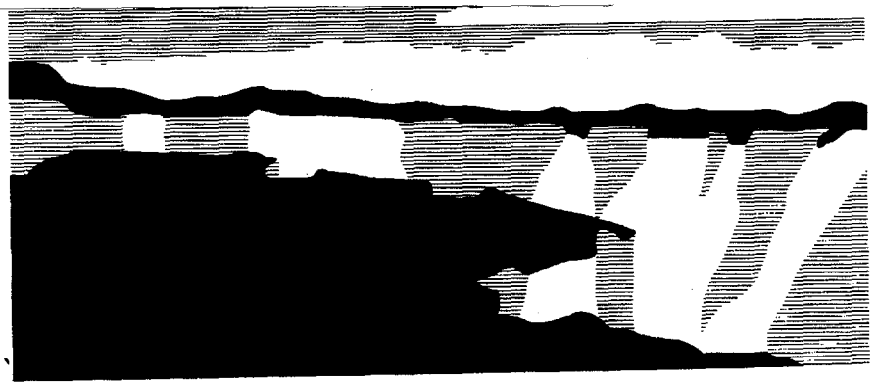

Los Alamos
NATIONAL LABORATORY

Form No. 836 R5
ST 2629 10/91

Materials Corrosion and Mitigation Strategies for APT: End of Year Report, FY '96

R. Scott Lillard, Darryl P. Butt

Materials Corrosion and Environmental Effects Laboratory
MST-6, Metallurgy
Los Alamos National Laboratory
Los Alamos, New Mexico 87545

submitted to:

Paul Lisowski
APT Project Office

October 30, 1996

contributors:

Doris K. Ford, Los Alamos National Laboratory, NMT-6

Gary Kanner, Los Alamos National Laboratory, MST-6

APT Materials Team:
Walter Sommer, MST-4
Stuart Maloy, MST-4
Gordon Willcut, TSA-10
Bob Brown, AOT-7
Eugene Zimmerman, AOT-7

Executive Summary

Our major accomplishment in FY '96 was the design and fabrication of the corrosion probes to be used "In Beam" during the FY '97 irradiation period to begin on February 1, 1997. Never before have corrosion rate measurements been made on-line in such a high radiation environment. To measure corrosion rate as a function of beam time, it is necessary to electrical isolate the corrosion electrode to be examined from the plumbing system. Conventionally, this is accomplished with glass seals. Here irradiation of the glass may cause it to become conductive, rendering the seal useless. To overcome this problem, the corrosion probes to be used in-beam at the spallation neutron cooling water loop at the LANSCE A6 target station were fabricated with ceramic inserts which act as electrical feed-throughs. The corrosion sample is joined to the ceramic by means of a compression seal. The corrosion samples are closed end cylinders, 0.5" diameter x 6.25" length, that are constructed from Stainless Steel 304L, Stainless Steel 316L, Inconel 718, Tungsten, HT-9, and Tantalum. Because of their specialized nature, InTa Corporation, of Santa Clara, CA was contracted to manufacture these probes. As of November 1, 1996 delivery of these probes has begun and we anticipate having all of the probes in hand by Nov. 25.

To examine the effects of long lived radiolysis products, corrosion probes will be placed at the top of the insert (down stream from the beam) away from the beam and high neutron flux regions. These probes are corrosion samples (rods; 0.125" diameter x 2" length) constructed from W, Ta, Al 6061, SS 304L, SS 316L, Inconel 718, Al 5052, and Al 6061. These samples are sealed in glass and joined to an NPT pipe plug style feed through. The pipe plug assembly is fitted to an in line "bucket" on the cooling water loop at the top of the insert. They will be capable of monitoring changes in the corrosion rates of that may result from differences in solution water chemistry, build up of water radiolysis products and, use of hydrogen water chemistry to mitigate corrosion. These probes, manufactured my Metal Samples Inc., of Munford AL, have been used in the past for this application and have met or exceeded all of our expectations. Delivery of the probes and electrodes is complete.

An alternate method for measuring the corrosion rate of tungsten and other metals in the proton beam is also being implement. This will be accomplished with weight loss measurements on foils measuring 2" x 5/16" x 1/16" made from W, SS 304L, SS 316L, Al 6061, Ta. These foils may be exposed directly to the beam or placed down stream depending on the availability of in-beam space. Weight loss is a direct method for calculating corrosion rate from the expression:

$$CR = \frac{543\mathrm{m}}{\rho \mathrm{A} \mathrm{t}}$$

where **CR** is corrosion rate in mils/yr, **m** is weight loss (initial - final) in milligrams, ρ is density in grams/cm^2, **A** is the exposed surface area in in^2 and, **t** is time of exposure in hrs.

The LANSCE A6 corrosion water loop will also be instrumented with a variety of probes aimed at determining the mechanism of corrosion including: pH probes, conductivity probes and, BWR reference electrodes. We will also investigate the efficacy of Hydrogen Water Chemistry used in BWR/PWR reactors to mitigate the formation of hydrogen peroxide (due to water radiolysis) on the LANSCE A6 corrosion loop. Hydrogen peroxide is a cathodic reactant and its build up in the loop can cause corrosion rates to increase by orders of magnitude The concentration of dissolved hydrogen in the water loop (being pumped in as a non-explosive mixture of Ar/H_2) will be monitored with a hydrogen gas analyzer manufacture by Orbisphere Labs, Inc. This same system is used by BWR/PWR reactors to evaluate the minimum concentration of dissolved hydrogen necessary to mitigate corrosion.

As of the date of this report (Nov. 1, 1997) all necessary preparation of the Corrosion Insert is on schedule for a February 1, 1997 date for beginning the irradiation.

During the fiscal year '96 we have also begun to characterize the corrosion electrochemistry of candidate APT target materials in simulated accelerator (laboratory) environments. These experiments have shown that hydrogen peroxide acts to increase the corrosion rate of tungsten by increasing the rate of the cathodic reaction. Because the anodic reaction rate (metal dissolution) must equal the cathodic reaction rate at the corrosion potential, the corrosion rate of tungsten is increased in peroxide. This report also presents data that shows the corrosion rate of machinable

tungsten (a two phase material: **a)** 99% W, **b)** 8.9 at% W, 21.4 at% Cu, 69.7 at% Ni) is more than 2 orders of magnitude greater than single phase 99.96% W. By far the most corrosion resistant target material is, however, is tantalum. The passive oxide which forms on Ta results in low passive current densities (less than $6x10^{-7}$ A/cm^2), immunity to pitting type corrosion (induced by chloride), and low corrosion current densities which result in lower corrosion rates when compared to tungsten for equal concentrations of hydrogen peroxide.

To characterize the passive film which forms on W, we have successfully employed Surface Enhanced Raman Spectroscopy (SERS). In this technique, small gold spheres (less than 50 nm in diameter) were electrodeposited onto a W electrode. This is done to "enhance" the otherwise undetectable low Raman signal produced by the 50 angstrom thick passive film on the tungsten surface. SERS experiments were then conducted on this electrode *in situ* as a function of applied potential and solution pH. The changes observed (as measured by SERS) correlated with what one would predict by thermodynamic calculations. In FY '97 we will use SERS and the baseline SERS data generated in FY '96 to evaluate the effects of radiation on passive film formation. This will be done in order that we may separate the effects of water radiolysis products from radiation effects on corrosion rate as measured on-line in the LANSCE A6 Target Station experiments. This will be accomplished by generating SERS data for W while being irradiated by an H^+ beam in the Blue Room at LANSCE. It is expected that any changes in the passive film due to irradiation will be observed in the SERS data.

In summary, the following primary tasks were complete in FY '96:

- Design / Fabrication of In-Beam Corrosion Probes
- Design / Fabrication of Out-of Beam Corrosion Probes
- Development of an On-Line pH Probe
- Literature Survey of Applicability of Hydrogen Water Chemistry to APT
- Development of an On-Line Conductivity Probe
- Literature Survey on Water Radiolysis Products: Production and Effects on Corrosion
- Conceptual Design for Instrumenting the A6 Corrosion Loop
- Acquired / Setup of Portable Corrosion Rate Measurements Systems for Use at the A6 Station
- Investigation of Applicability of BWR Reference Electrodes to APT
- Literature Survey on the Effects of Hydrogen Peroxide on Corrosion
- Baseline Corrosion / Electrochemistry on W and Ta in Hydrogen Peroxide
- Baseline Corrosion / Electrochemistry on W as a function of applied potential and solution pH
- Literature Survey on Tungsten Corrosion
- Effects of pH on the Corrosion / Electrochemistry of W
- Literature Survey on Surface Enhanced Raman Spectroscopy
- Literature Survey on Traditional Raman Spectroscopy of Tungsten Oxides
- *In Situ* Examination of Oxide Formed on Tungsten with Surface Enhanced Raman Spect.

not reported on here:

- Lead Corrosion in Hydrogen Peroxide using a Rotating Disk Electrode
- Corrosion of Braze Material in Nitric Acid and Hydrogen Peroxide

Table of Contents

List of Tables

List of Figures

List of Equations

Introduction

The focus of our efforts in Fiscal Year 1996 was on the corrosion measurements at the LANSCE A6 target station to begin on February 1, 1997. Our Implementation Plan for these experiments calls for in-beam corrosion probes to measure the real-time effects of proton irradiation on the corrosion rate of neutron spallation target and structural materials. The design and construction of probes to measure corrosion rates of these materials while being irradiated by an 800 MeV proton beam has been a major challenge as no commercially available probes are designed to withstand the anticipated high proton and neutron fluxes. The component most susceptible to radiation damage is the insulating material which electrically isolates the corrosion probe from the stainless steel cooling water loop. Commercially available probes incorporate glass seals to provide electrical isolation. However, glass is susceptible to irradiation damage and consequently becomes conductive thus compromising its efficiency as an electrical insulator. As discussed below, we have designed a ceramic seal to overcome this problem. From the surface this may appear to be a simple problem. Unfortunately, there is a large mismatch in the coefficient of thermal expansion between ceramics and the metals of interest which leads to fabrication difficulties. For example the coefficient of thermal expansion for tungsten is 0.016 ppm/K and that of 316L stainless steel is 17 ppm/K while the thermal coefficient of expansion for alumina is approximately 7 ($x10^{-6}$/K; at room temperature). Thus, fabrication of corrosion probes to measure the real-time corrosion rate of materials while being irradiated has been a significant development project.

In addition to the "in-beam" corrosion probes at the LANSCE A6 target station, the cooling water loop will also be instrumented with out-of-beam corrosion probes and u-bend stress corrosion cracking (SCC) samples to evaluate the effects of water radiolysis and changes in the water chemistry on corrosion rate. While u-bend type SCC samples require visual examination after the irradiation period, the out-of-beam corrosion probes will allow us to make accurate real time measurements. To investigate the mechanism for the changes in corrosion rate, conductivity probes, reference electrodes, and pH probes will also be placed on both the inlet and outlet sides of

the cooling water (relative to the beam) at the top of the insert, i.e., far away from the beam spot. The effects of long lived water radiolysis products on corrosion potential and solution pH will be directly monitored at these positions. Because it is necessary to maintain a chloride free environment in the cooling water loop, and radiation damage to traditional reference and pH electrodes may cause a release of concentrated chloride solution, specially designed reference and pH electrodes are necessary. As detailed in this report, corrosion potential measurements will, therefore, be made with commercially available electrodes designed for use in boiling water reactors. Solution pH measurements will be made with an experimental tungsten/tungsten oxide electrode. Lastly, the concentration of metal species in solution at the LANSCE cooling water loop will be monitored *ex situ* with ion coupled plasma. This necessitates that water samples be removed from the cooling water loop periodically. These samples will also be checked for hydrogen peroxide concentration (a water radiolysis product).

In addition to corrosion rate measurements, mitigation strategies will be tested during the LANSCE A6 target station irradiation experiments. As discussed below, the water radiolysis product having the highest concentration after a few milliseconds is hydrogen peroxide (H_2O_2), an oxidizing agent. To limit the increase in corrosion rate which results from hydrogen peroxide, we will employ so called Hydrogen Water Chemistry (HWC). In HWC, hydrogen gas is bubbled into the cooling water loop upstream from the proton beam spot which results in dissolved atomic hydrogen in the cooling water. It is this dissolved atomic hydrogen which limits hydrogen peroxide formation as will be described in more detail below.

Water Radiolysis Radiolysis models **[1,2,3]** have found that both oxidizing and reducing species are produced when water is irradiated with proton, neutron, or gamma radiation. While this includes many radicals, the species having the highest concentration after a few milliseconds is hydrogen peroxide (H_2O_2)**[4]**. Hydrogen peroxide, an oxidizing agent, is formed from the combination of two OH radicals produced during irradiation:

$$OH + OH \xrightarrow{k_{H_2O_2}} H_2O_2 \quad k_{H_2O_2} = 4x10^9 \text{ /(mol sec)} \qquad \text{Eq. 1}$$

In cases where the rate of the corrosion reaction is cathodically limited, the formation of peroxide can be particularly detrimental as its presence and products which result from its decomposition (namely O_2), will increase the rate of the cathodic reaction. As a consequence, in a positive shift in the open circuit potential[**5**] and an increase in the corrosion rate[**6,7**] is observed. We believe that hydrogen peroxide formation can be mitigated in the neutron spallation target cooling loop by using Hydrogen Water Chemistry (HWC)[**8,9,10,11**] currently used in operating commercial boiling water reactors. By bubbling H_2 gas into the cooling water the OH radical preferentially reacts with dissolved (atomic) hydrogen to form water according to the reaction:

$$OH + H \xrightarrow{k_{H_2O}} H_2O \quad k_{H_2O} = 2.4\text{x}10^{10} \text{ mole/sec} \qquad \text{Eq. 2}$$

While some valuable insight into the effects of radiolysis products on corrosion rates has been gained through laboratory simulation[**12**], many of the radiolysis products are short lived and difficult or impossible to reproduce in the absence of a high energy radiation source. Therefore, a method for measuring the corrosion rates of candidate materials in a prototypical cooling water loop is preferable. To successfully measure the corrosion rate of the proposed materials in a cooling water loop irradiated by a proton beam the measurement system must have the following attributes: 1) because the solution resistance will be very high the method must allow this resistance to be accounted for, 2) in order to monitor only the effects of the cooling water loop on corrosion rate the method should be non-destructive 3) because the plumbing would act as an electrical sink for a traditionally grounded instrument the measurement system must be isolated from ground (referred to as a "floating ground"), and 4) the measurement system should be portable to allow it to be easily moved from location to location.

Electrochemical Measurements The cooling water in the LANSCE A6 corrosion loop is distilled and de-ionized prior to being pumped into the system. It has an initial resistivity of approximately 10^6 (ohm cm). Therefore, the resultant solution resistance between two parallel plate electrodes 1 cm^2 in area and separated by 1 cm in this solution would be 10^6 ohms. In traditional dc electrochemical techniques for measuring corrosion rate, the solution resistance (R_{sol})

can be neglected if it is small relative to the polarization resistance (R_{pol} which is inversely proportional to corrosion rate); i.e. $V_{applied}/I_{meas} = R_{meas} = R_{sol}+R_{pol}$. Typical values for R_{sol} are on the order 100 ohms or less as compared to R_{pol} which is generally on the order of 10^6 ohms. Because R_{sol} in the LANSCE A6 water loop is large, if not corrected for, the polarization resistance will be over estimated and, as a result, the corrosion rate will be underestimated.

Electrochemical Impedance Spectroscopy (EIS) is a powerful non-destructive technique for measuring the corrosion rates of metals in aqueous environments**[13,14,15]** and is ideally suited for systems with high solution resistivity. In EIS a small sinusoidal voltage perturbation (10 - 30 mV) is applied across the sample interface as a function of frequency. By measuring the transfer function of the applied ac voltage perturbation and the ac current response of the material, an impedance results ($Z\omega=V\omega/I\omega$). In the simplest sense, at low frequencies the material behaves as a resistor and $Z\omega=(R_{sol}+R_{pol})$. At high frequencies, the material behaves as a capacitor and, therefore, offers no resistance to current. As a result $Z\omega=R_{sol}$. By measuring $Z\omega$ over a wide frequency range the solution resistance can be subtracted from the polarization resistance. Because the ac voltage perturbation used in EIS is small, it is a nondestructive technique and corrosion rates can be measured at the material's "free corrosion potential" (i.e. its open circuit potential).

Surfaced Enhanced Raman Spectroscopy Materials (W, Inconel 718, SS 304L) exposed to the proton beam in the APT target blanket cooling water loop may suffer accelerated corrosion damage due to water radiolysis products, oxide irradiation damage, or a combination of both. To separate out the effects of oxide damage due to irradiation from those induced by water radiolysis, an *in situ* method for characterizing the passive oxide formed on these materials before, during, and after irradiation is desirable. One technique for characterizing *in situ* changes in the oxide film is Surface Enhanced Raman Spectroscopy (SERS).

Because the intensity of Raman signals are inherently weak (i.e. "bulk concentrations" are typically required), traditional Raman spectroscopy is not suitable for analyzing the passive oxides formed on metals as these films are generally less than 5 nm in thickness. Researchers investigating adsorption on metals have found that gold substrates enhanced the Raman signal from

adsorbates and hydroxides even for those layers which were only a few angstroms in thickness[16,17]. This enhancement is not well understood, but has been attributed to either chemical[18] or electromagnetic effects[19]. More recently, investigators have found that the electrodeposition of noncontinuous silver[20,21,22,23] or gold[24] spheres (less than 50 nm in diameter) onto the native oxides formed on Ni and Fe will also produce a Raman enhancing effect. Because the passive oxide produces a unique signal which is related to hydration, structure (i.e. co-ordination of atoms), and composition, the SERS signal from a sample immersed in solution can easily be separated from those of the aqueous environment. Further, any changes in the oxide due to irradiation, polarization, etc. are measurable.

Summary of Accomplishments in FY '96

Design and Fabrication of the Corrosion Loop at the LANSCE A6 Target Station

Configuration / Instrumentation of the Corrosion Loop A diagram representing the A6 Corrosion Loop is presented in Figure 1. Full engineering diagrams for the corrosion insert and its pumping system can be found in Appendix A and B respectively. This will be a closed loop system, filled with de-ionized water. Each of the diagnostics in this figure are detailed in the following sections. The primary diagnostics for evaluating the corrosion rates of candidate APT materials are represented in this figure as "out-of-beam corrosion" and "in-beam corrosion". The out-of-beam designation refers to samples placed in the supply stream and return stream of the flow line to evaluate the effects of long lived radiolysis products on the corrosion rates of materials. The in-beam designation refers to corrosion probes that will be placed directly in the proton beam to evaluate the effects of the beam as well as short lived radiolysis products on the corrosion rates of candidate materials. The in-beam area is shown in greater detail in Figure 2.

In an attempt to evaluate the combined effects of load and corrosion stress corrosion cracking samples (designated as SCC) will also be placed in the flow stream. These samples will be placed below the insert to allow exposure to a high flux of neutrons as shown in Figure 2. They consist of small u-bend specimens in accordance with ASTM standard G30-79[25].

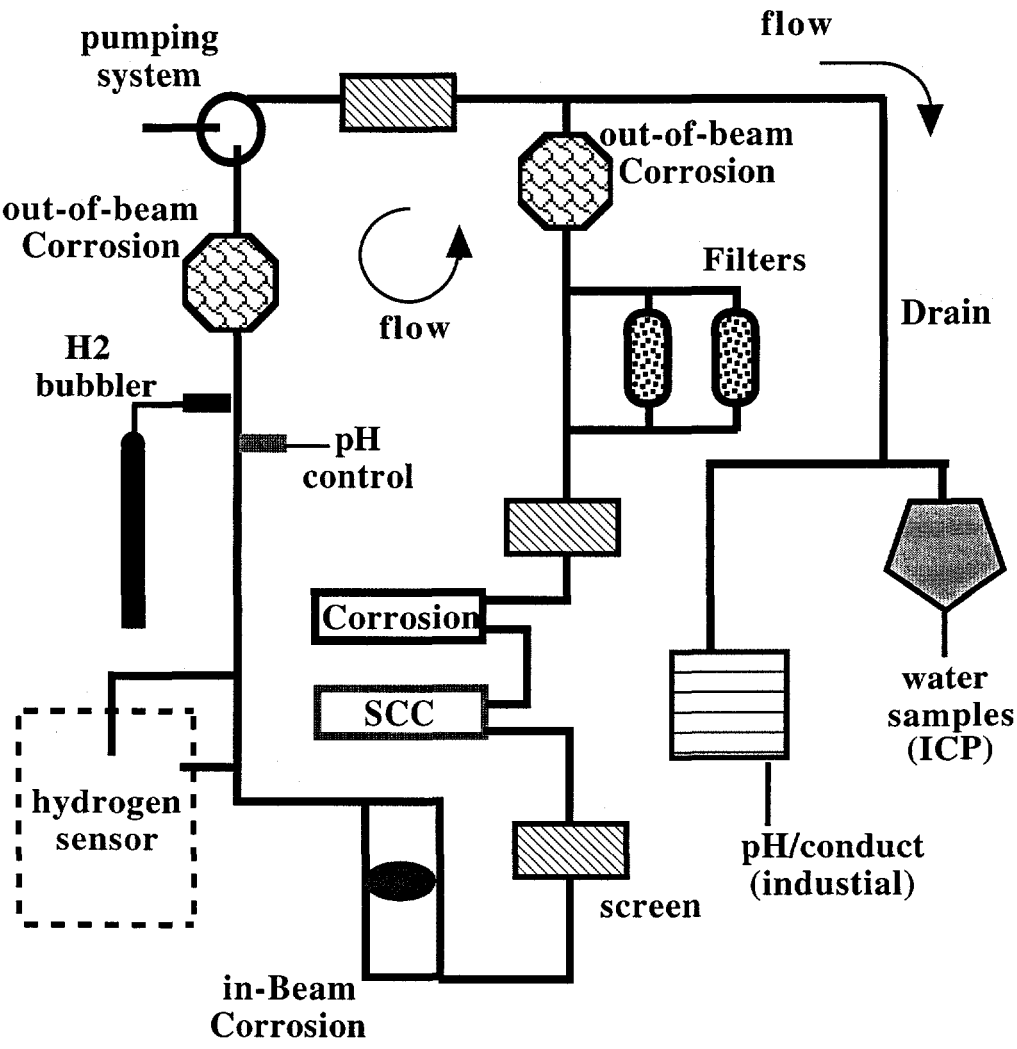

Figure 1 A diagram representing the corrosion diagnostics to be used on the cooling water loop at the LANSCE A6 target station. The proton beam is perpendicular to the diagram and is represented by the orange oval over top the in-beam corrosion probes

To mitigate corrosion, hydrogen gas will be bubbled into the flow stream (designated as H_2 bubbler) as done in the BWR/PWR community. To monitor the concentration of dissolved hydrogen in the flow stream a commercial hydrogen sensor will be placed in the flow loop. In addition to commercially available pH and conductivity probes placed in the drain line of the water system the probes designed for measuring pH and conductivity in a high radiation environment will be placed directly in the cooling water loop. In the event that it is necessary to adjust the pH of the cooling water system, a dosing pump for small additions of LiOH or HNO_3 will be placed on this system. A commercially available reference electrode (approved by the NRC and used by the

PWR / BWR community) will also be placed in the return stream of the water system. This electrode will be used to monitor the corrosion potential of the samples in the return stream as a function of time.

In Beam Corrosion Probes One of our major goals for FY '96 was the design and fabrication of the corrosion probes to be used "In Beam" during the FY '97 irradiation period to begin on February 1, 1997. To measure corrosion rate as a function of beam time, it is necessary to electrically isolate the corrosion electrode from the cooling water loop. Conventionally, this is accomplished with glass seals. However, irradiation of the glass may cause it to become conductive, rendering the seal useless. To allow us to measure corrosion rates directly in an 800 MeV proton beam operating at 1 mA, an alternate sealing method was chosen as described below.

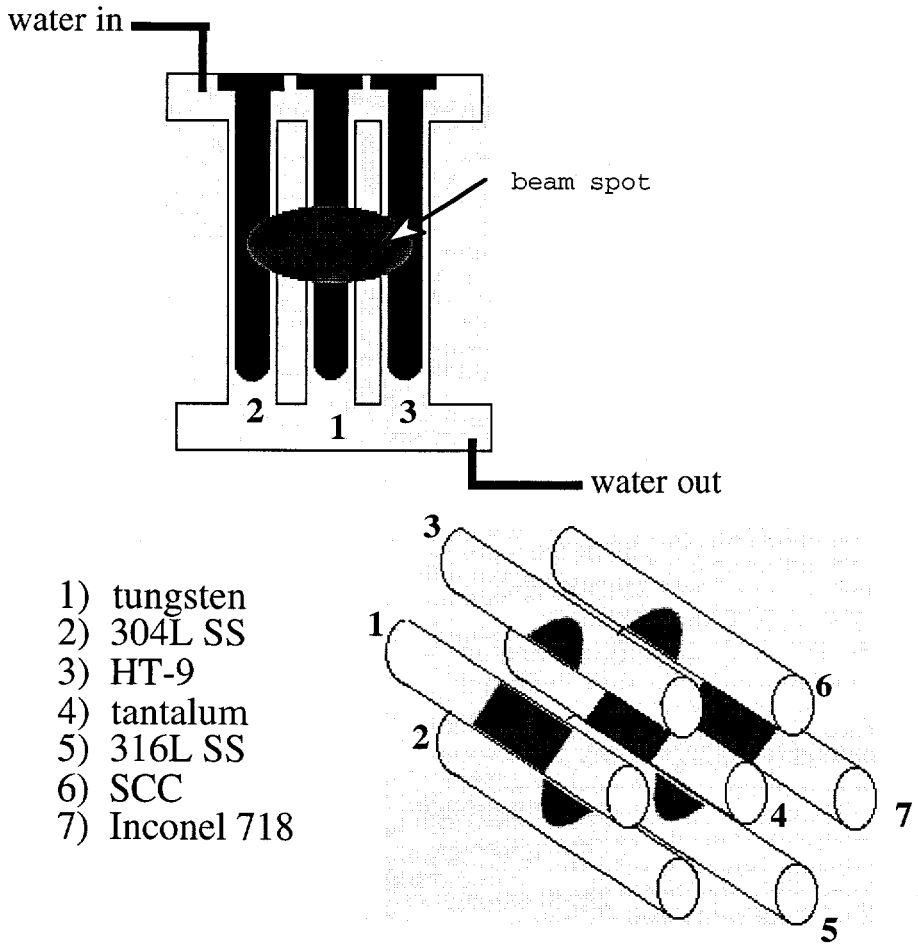

Figure 2 A diagram representing the placement of the in beam corrosion probes to be used on the cooling water loop at the LANSCE A6 target station. The orange oval represents the approximate beam location.

The corrosion probes to be used in-beam at the spallation neutron cooling water loop at the LANSCE A6 target station consist of ceramic inserts which act as electrical feed-throughs. The corrosion sample is joined to the ceramic by means of a compression seal. This design is shown in Figure 3. The corrosion samples are cylinders (1 end closed), 0.5" diameter x 6.25" length, that are constructed from Stainless Steel 304L, Stainless Steel 316L, Inconel 718, Tungsten, HT-9, and Tantalum. Because the expansion coefficients of these materials vary widely, no one ceramic

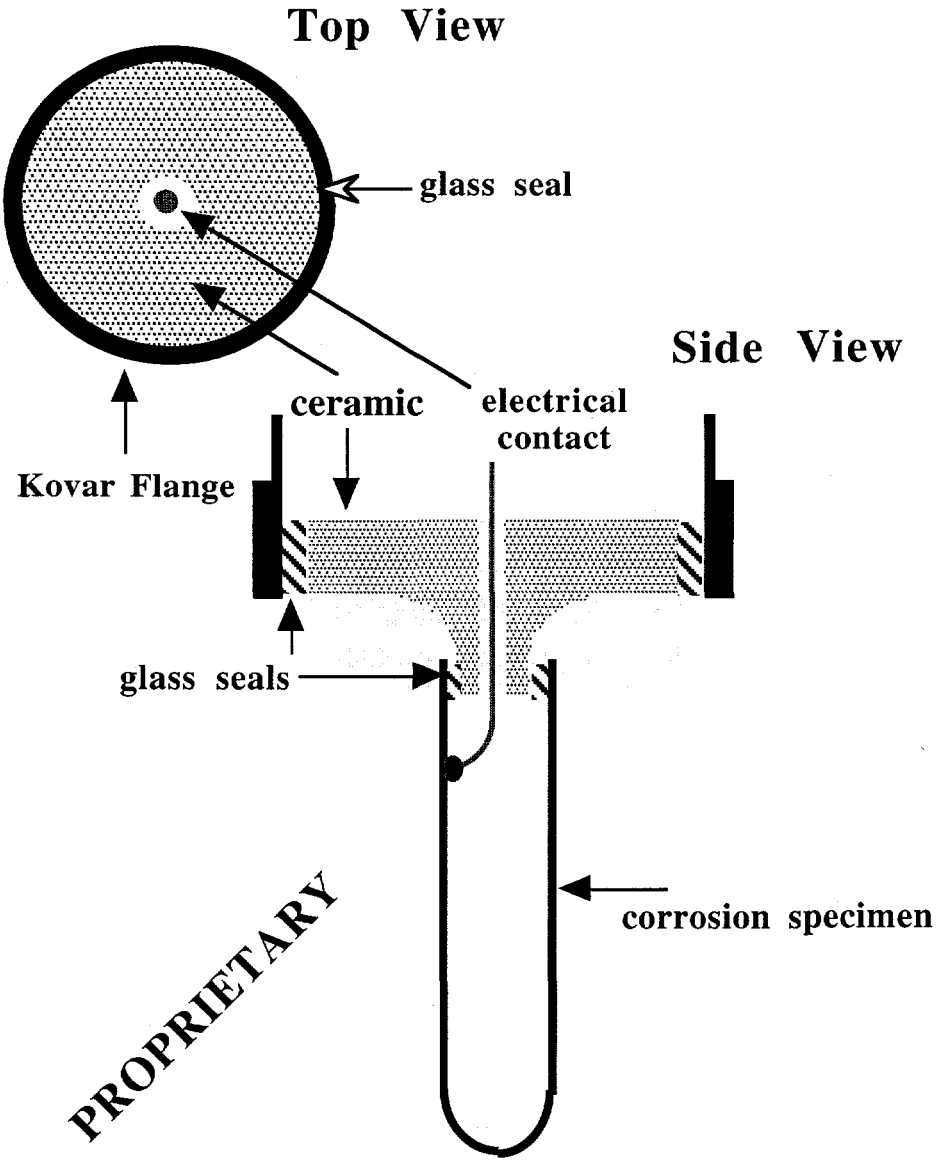

Figure 3 In beam corrosion probe to be used in spallation neutron cooling water loop at the LANSCE A6 target station.

is capable of holding the compression seal without cracking. The corrosion samples with high expansion coefficients (304L, HT-9, I718, 316L) were joined to the feed-through with alumina. Those with low expansion coefficients (W, Ta) were joined with silicon nitride. These feed-throughs will be welded to a manifold (using weld flanges which are made of Kovar or SS 304L) at the base of the corrosion insert at the Area 6 Target Station in such a manner to allow direct exposure of the electrode to the proton beam for real-time measurement of corrosion rates by Electrochemical Impedance Spectroscopy. Because of their specialized nature, InTa Corporation, of Santa Clara, CA has been contracted to manufacture these probes. As of November 1, 1996 delivery of these probes has begun and we anticipate having all of the probes in hand by Nov. 25.

An alternate method for measuring the corrosion rate of tungsten and other metals in the proton beam is also being implemented. These efforts focus on weight loss measurements of 2" x 5/16" x 1/16" foils made from W, SS 304L, SS 316L, Al 6061, and Ta. These foils may be exposed directly to the beam or placed down stream depending on the availability of in-beam space. Weight loss is a direct method for calculating corrosion rate from the expression:

$$CR = \frac{543\mathrm{m}}{\rho \mathrm{At}} \qquad \text{Eq. 3}$$

where **CR** is corrosion rate in mils/yr, **m** is weight loss (initial - final) in milligrams, ρ is density in grams/cm^2, **A** is the exposed surface area in in^2, and **t** is time of exposure in hrs.

The weight loss specimens will be held in individual SS 304L baskets which will allow direct exposure to the beam and the cooling water (Figure 4). The foil (W, Ta, SS 304L, SS 316L, I 718, and Al 6061) is held in place by screwing the two basket halves together to hold the sample in place. This will also allow easy removal of the sample after the irradiation period. These baskets will be held in the proton beam center-line by welding into the identical manifold designed for the ceramic-seal corrosion probes as shown in Figure 5.

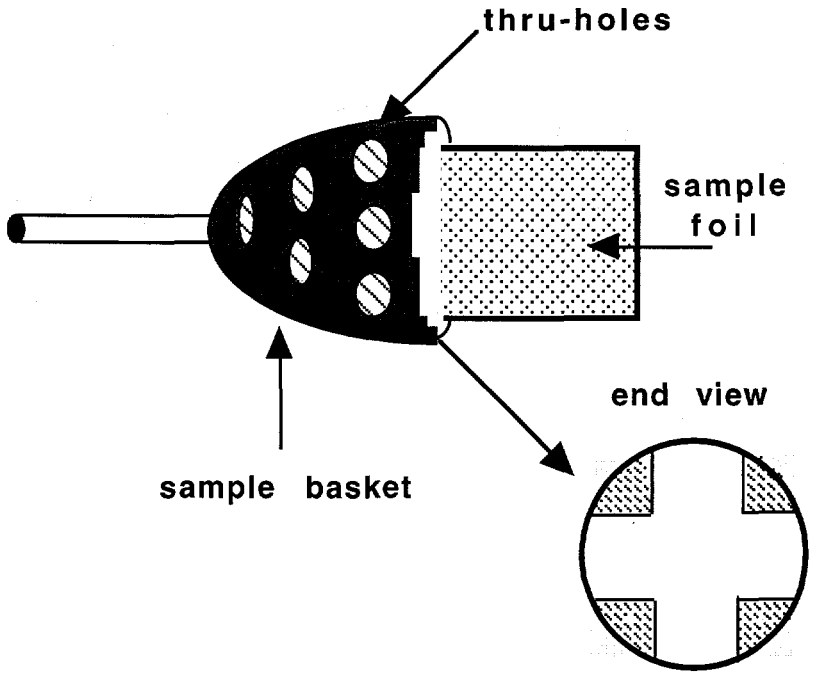

Figure 4 Diagram of the sample basket that will be used to hold the weight loss samples used to measure corrosion rate "in-beam".

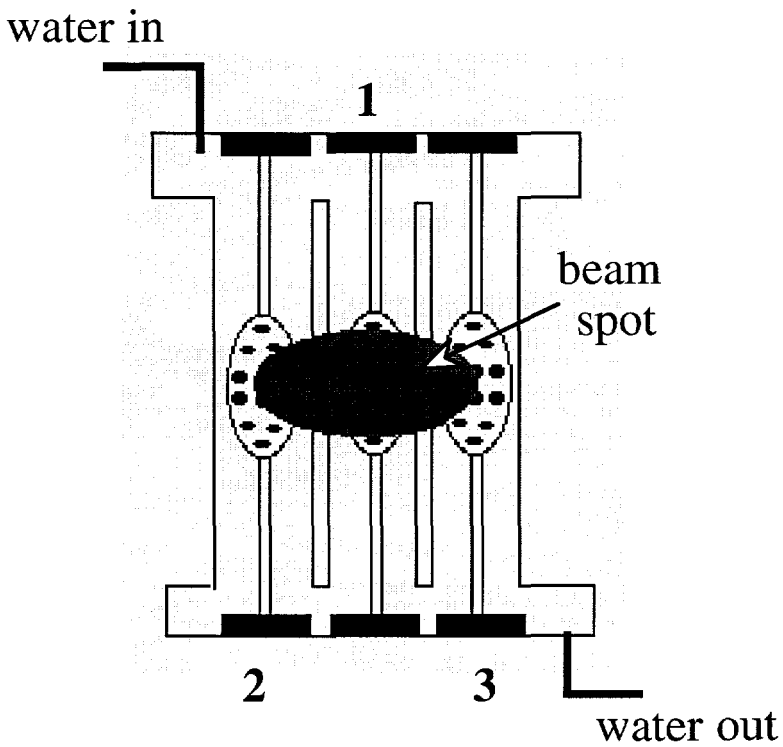

Figure 5 Diagram depicting the manifold and manner in which the specimen baskets (Figure 4) will be held in the beam center line.

Out of Beam Corrosion Probes The corrosion probes to be used out-of-beam in the LANSCE corrosion experiments were fabricated from samples (rods' 0.125" diameter x 2" length) of the same materials described in the in-beam experiments as well as Aluminum 6061 (Figure 6). These samples are seated onto studs which are sealed in glass and joined to an NPT pipe plug style feed through. The pipe-plug assembly is fitted to an in-line corrosion cell (constructed from SS 304L) on the cooling water loop at the top of the insert. This will allow us to monitor changes in the corrosion rates of W, Ta, Al 6061, SS 304L, SS 316L, Inconel 718, and Al 5052 that result from differences in solution water chemistry. These anticipated changes will be correlated with increased beam current, build up of water radiolysis products, and the use of hydrogen water chemistry to mitigate corrosion.

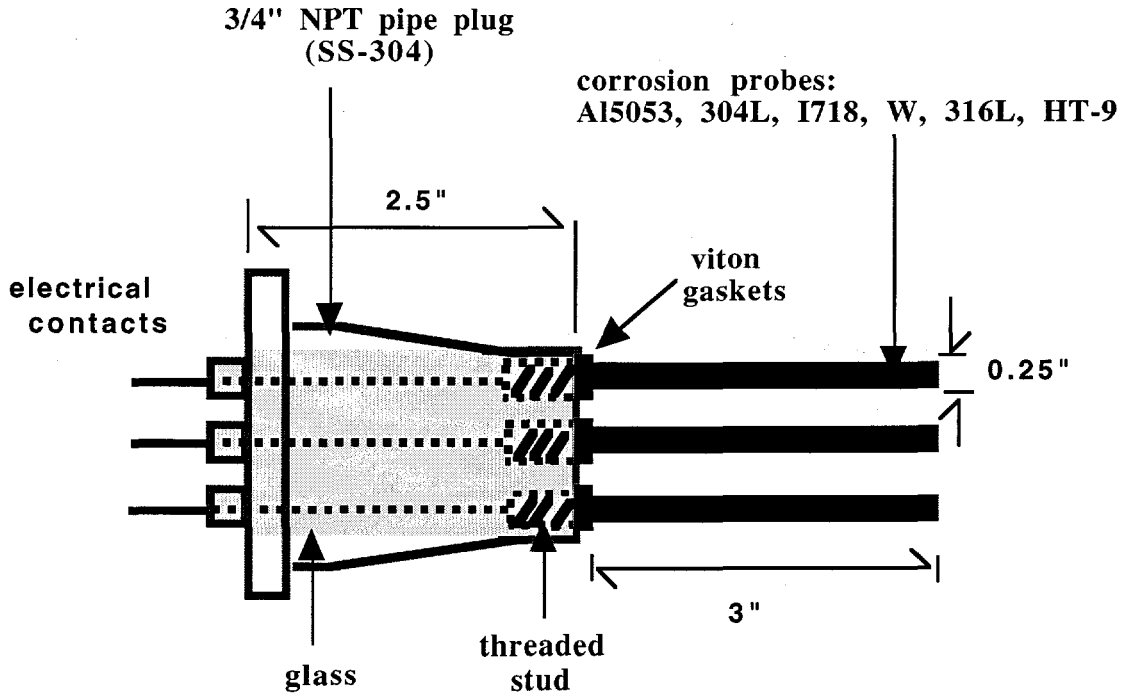

Figure 6 Out of beam corrosion probe to be used in spallation neutron cooling water loop at the LANSCE A6 target station.

We have used the NPT feed throughs, manufactured by Metal Samples Inc., of Munford, AL, in the past for this application[**28**]. These probes have met or exceeded all of our expectations. Delivery of the probes and electrodes is complete.

pH Probe Development To monitor the pH of the cooling water, we have tested a tungsten/tungsten oxide electrode used in commercial BWR's for the same purpose. It has been demonstrated[**26**] that the potential of a tungsten/tungsten oxide electrode shows a Nernstian pH response. In our work, we have found the relationship between the open circuit potential (OCP) of the tungsten/tungsten oxide electrode and solution pH to be:

$$E = 0.08 - (0.030)pH \qquad \text{Eq. 4}$$

as shown in Figure 7. This figure was generated by measuring the OCP of a tungsten /

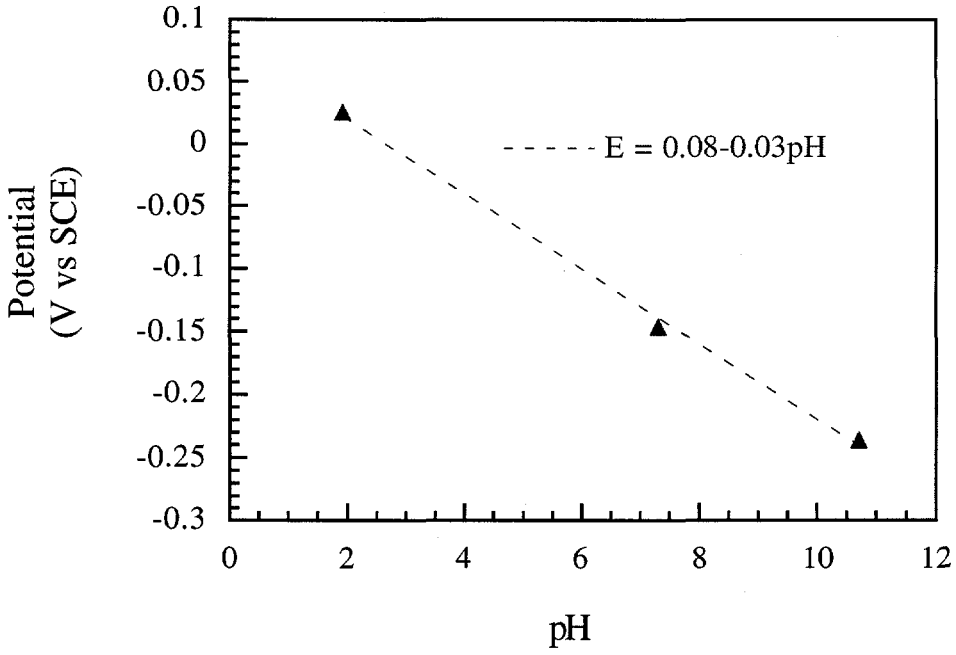

Figure 7 Variation in the OCP of a tungsten/tungsten oxide electrode vs SCE as a function of solution pH.

tungsten oxide electrode vs Saturated Calomel (SCE) in three separate buffer solutions: 0.25M tartaric acid, pH 1.97; 0.5M boric acid/0.05M sodium borate. pH 7.2; 0.25M sodium

borate/sodium hydroxide pH 10.5. This electrode is easily fabricated by the high temperature oxidation of tungsten in an oxygen containing environment and can be attached directly to the out-of-beam corrosion probes to be used at LANSCE (Metal Samples, Inc.). Furthermore, this electrode is insensitive to changes in dissolved hydrogen concentration unlike a platinum electrode (Figure 8). Unfortunately, some variation in the OCP of the tungsten/tungsten oxide electrode

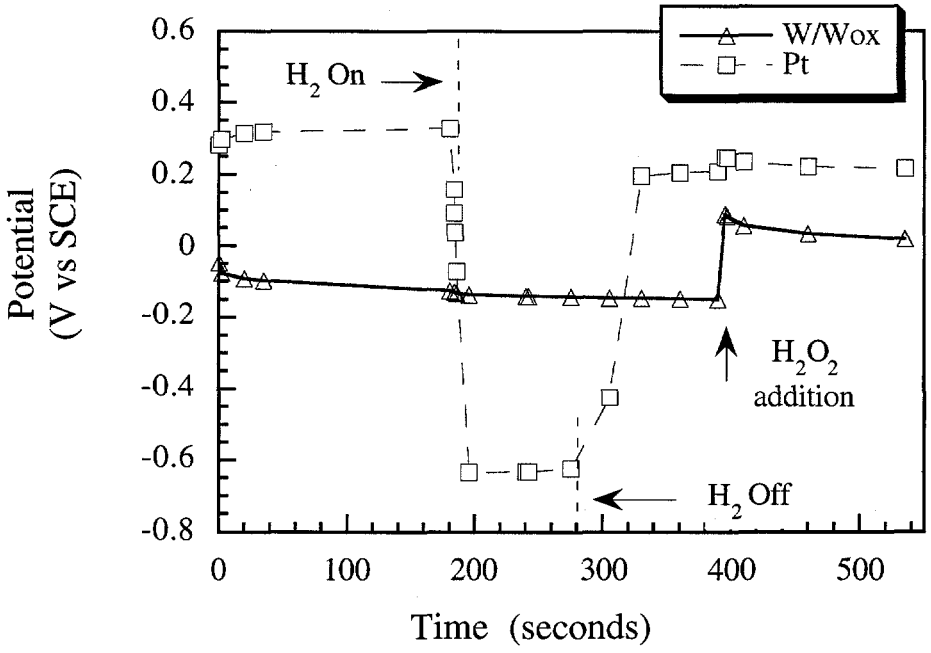

Figure 8 Variation in the OCP of tungsten/tungsten oxide and platinum electrodes vs SCE in pH 7 buffer solution as a function of dissolved hydrogen and hydrogen peroxide additions.

was observed upon the addition of high hydrogen peroxide concentrations (also shown in Figure 8). Therefore, the tungsten/tungsten oxide electrode will only be used to make solution pH measurements while hydrogen water chemistry (HWC) is being implemented to mitigate the formation of hydrogen peroxide. To measure the cooling water pH during periods when HWC is not being employed, an industrial process pH probe placed in the drain line will be used. This probe is not placed in the main cooling water loop as it is constructed from glass and PTFE and mechanical failure of the probe would result in dumping several milliliters of saturated potassium chloride solution into the cooling water system.

Reference Electrode / Conductivity Probes To measure changes in the open circuit potential of the out-of-beam samples as a function of water irradiation (time), a reference electrode was purchased. This electrode, manufactured by NWT Associates, San Jose, CA, (model NWT R201, Air Cooled High Temperature, High Pressure External Reference Electrode) was designed for the nuclear power industry and tested in both PWR and BWR reactors**[27]**. This design incorporates a porous zirconia frit and an aluminum finned cooler to compensate for elevated system pressure and temperature. The half reaction is that of Ag/AgCl in dilute potassium chloride solution (10^{-5}M KCl), thus eliminating any consequences from contamination of the cooling water loop with the electrode solution if the probe is damaged

Conductivity probes were fabricated at LANL from the three electrode out-of-beam corrosion probes presented in Figure 6 (Metals Sample, Inc.). They were constructed by welding a hollow SS 304 tube onto two of the feed through studs. This stainless steel sleeve surrounds a small stainless steel rod (also made from SS 304) which is welded onto the third feed through stud (Figure 9). This geometry allows the probe cell constant (used to convert solution resistance to resistivity) to be determined more accurately than the configuration used in earlier experiments on the LANSCE XO2 cooling water system**[28]**. One of these probes will be placed in both the supply and return streams at the top of the corrosion insert .

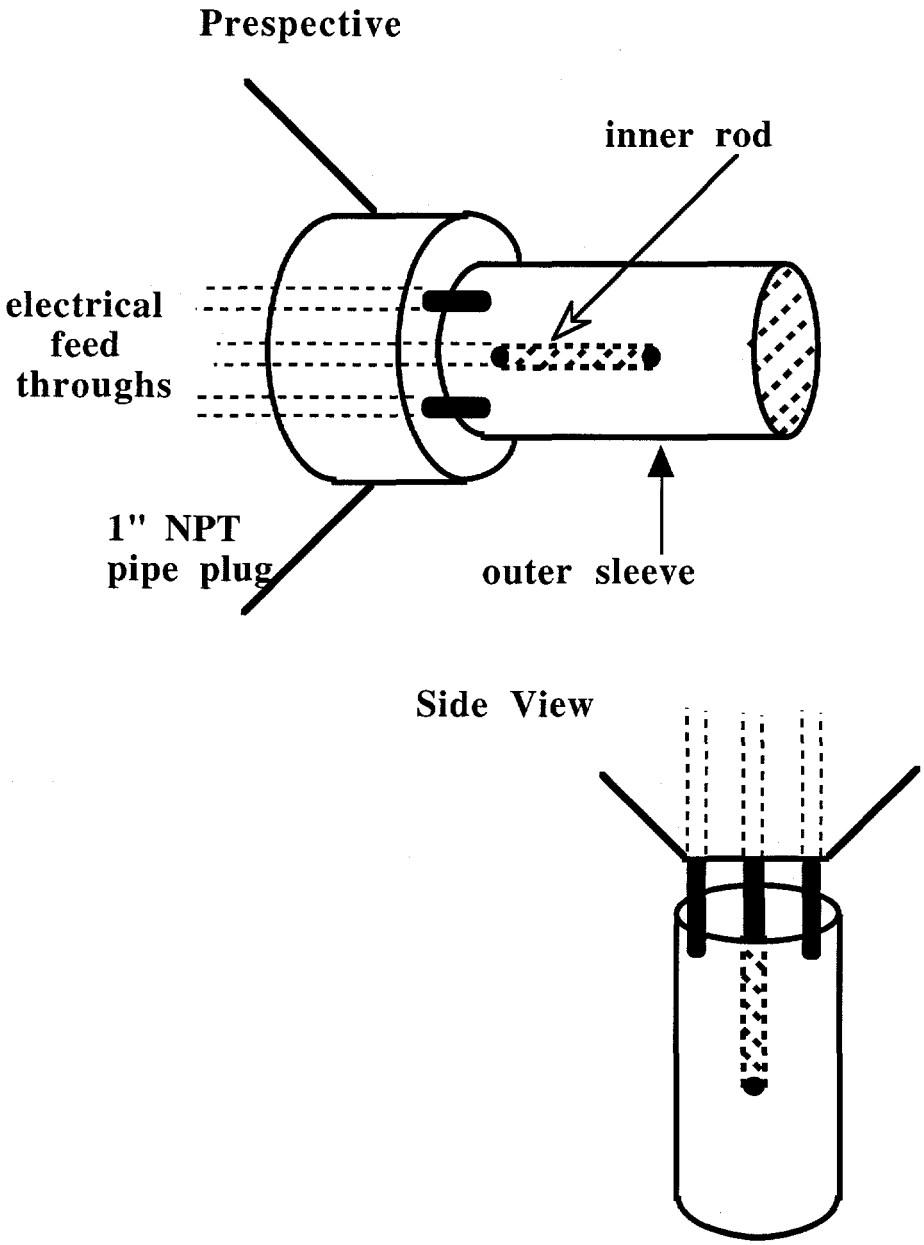

Figure 9 Diagram of the probes to be used to measure solution conductivity during the LANSCE corrosion irradiation experiments.

Corrosion Mitigation: Hydrogen Water Chemistry In an attempt to mitigate the formation of hydrogen peroxide, Hydrogen Water Chemistry used in boiling water reactors will be implemented during the LANSCE irradiation experiments. This will be accomplished by bubbling a mixture of H_2 / 94% Ar gas directly into the water loop, ahead of the proton beam-spot. The dissolved hydrogen concentration in the cooling water loop during the LANSCE irradiation

experiments will be monitored with a remote hydrogen sensor, Orbisphere Laboratories, Emerson NJ, (model #3610/220.E, TCD Hydrogen Gas System). The efficacy of HWC will be evaluated by monitoring the corrosion rates of the in-beam and out-of-beam corrosion samples as well as the OCP of the out-of-beam probes with the NWT Ag/AgCl reference electrode. As discussed earlier the OCP increases with increasing H_2O_2 concentration. It has been shown for BWR / PWR reactors that the OCP is greatly suppressed during HWC**[9,11,29,,30,31,32,33,34,35]**. Moreover, as demonstrated in the following sections of this report, hydrogen peroxide is a cathodic reactant. Therefore, minimizing its concentration should lower corrosion rates. It is for this reason that we feel HWC will be critical in minimizing corrosion rates and extending the life-time of the target and structural materials used in the APT accelerator.

Laboratory Experiments

This section details the progress we have made in the laboratory during FY '96. The goal of these experiments is to establish baseline data for comparison with the corrosion measurements to be made during the FY '97 irradiation at the LANSCE A6 Target Station Corrosion Loop. It consists of work in two major areas: 1) traditional dc electrochemistry in simulated APT environments and 2) Surface Enhanced Raman experiments.

Experimental The samples evaluated in this study were fabricated from 99.96% Ta and three grades of tungsten: 1) 99.96% W, 2) 99% W, and 3) two phase machinable tungsten: **a)** 99% W; 8.9 at% W and **b)** 21.4 at% Cu, 69.7 at% Ni. Scanning electron micrographs for 99.96% W and machinable W are presented in Figure 10 and 11, respectively. The two phase structure of the machinable tungsten is easily identified in Figure 11 as a dark phase.

After making electrical contact, each sample was mounted in epoxy and ground with successively finer grits of SiC paper and finished with alumina on a polishing wheel. The final mechanical polish being 0.3 μm alumina. In some cases this was followed by a chemi-mechanical polish on the polishing wheel with colloidal silica (0.06 μm, pH=10).

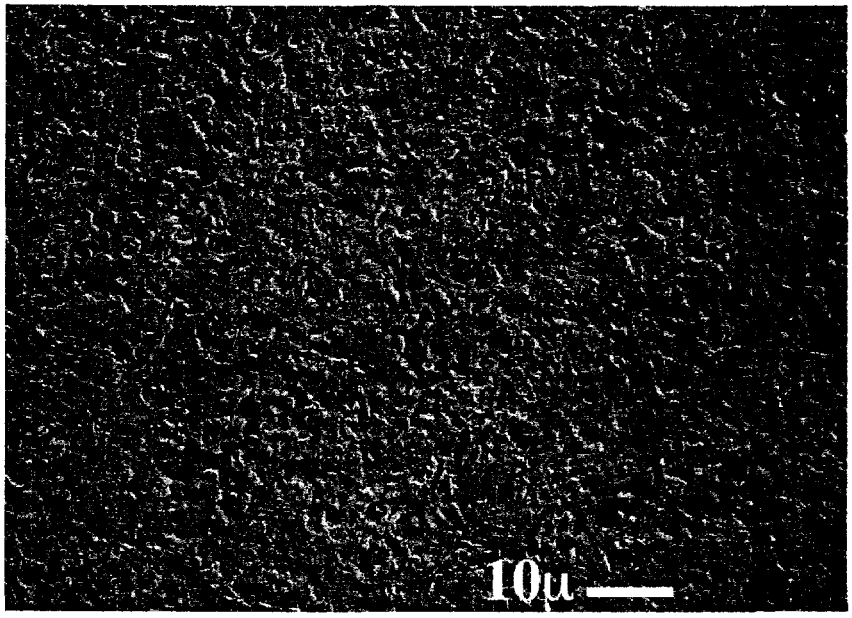

Figure 10 SEM micrograph of the 99.95% tungsten target sample after polishing. The surface had a modeled appearance.

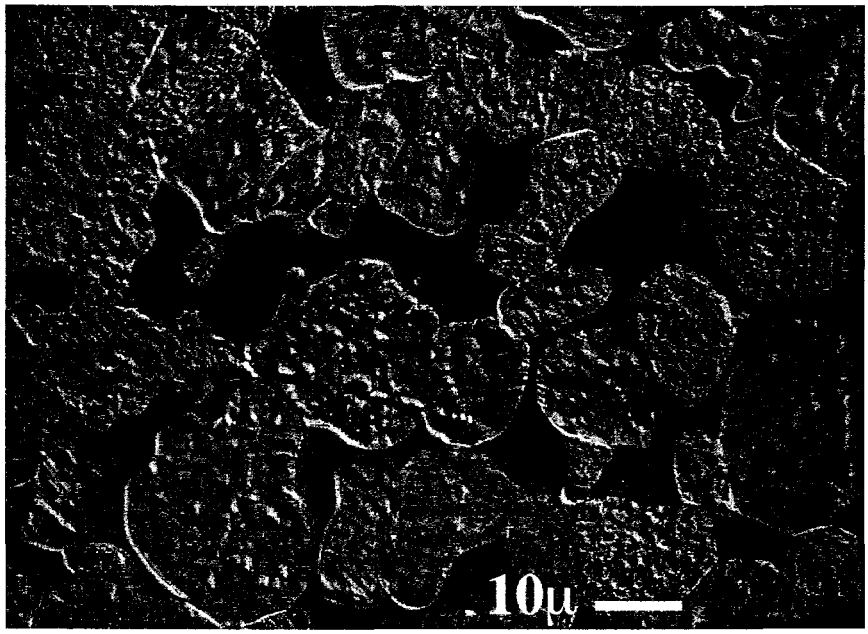

Figure 11 SEM micrograph of the machinable tungsten sample formerly used as a target material at LANSCE. Dark phase is rich in Ni/Cu while the light phase is relatively pure tungsten.

The solutions used in this investigation consisted of: 1) 0.10M NaCl, 2) 0.0M H_2O_2, and buffer solutions with and without 0.10M NaCl: 4) 0.25M tartaric acid (pH 1.9), 5) 0.50M boric acid / 0.05M sodium borate (pH 7.2) and, 6) 0.25M sodium borate / sodium hydroxide (pH 10.6). All solutions were made with reagent grade chemicals and distilled / deionized water. As noted in the text, some solutions were deaerated with ultra high purity argon for 18 hours prior to immersion of the sample while others were bubbled with laboratory air. For solutions which contained chloride, a Saturated Calomel reference Electrode (SCE; +0.242V vs NHE) was used. For those solutions not containing chloride, a Mercury / Mercury Sulfate reference Electrode (MMSE; +0.640V vs NHE) was used to prevent contamination of the solution. For the sake of clarity, all potentials are referenced vs SCE independent of the reference electrode that was used.

Potentiodynamic polarization curves were generated at a scan rate of 0.1mV / sec in the potential region between -0.100V vs OCP (Open Circuit Potential) and approximately +1.4 V vs SCE. These curves were generated after 1 hour at the OCP to allow steady state to be achieved.

Surface Enhanced Raman experiments were generated with an Ar^+ pumped Ti-sapphire laser. The wavelength was tuned to 715 nm and a power approximately 50 $x10^{-3}$ watts was used. The spot size was approximately 200 μm in diameter. Data were collected over the range of 200-1200 cm^{-1} and calibrated with respect to the neon line spectrum. Prior to SERS experiments a thin, discontinuous layer of gold spheres, measuring approximately 50 nm in diameter (Figure 12), was electrodeposited onto each sample surface from a quiescent 0.01M $AuCl_3$ solution, at approximately 30 $x10^{-3}$ Coulombs / cm^2.

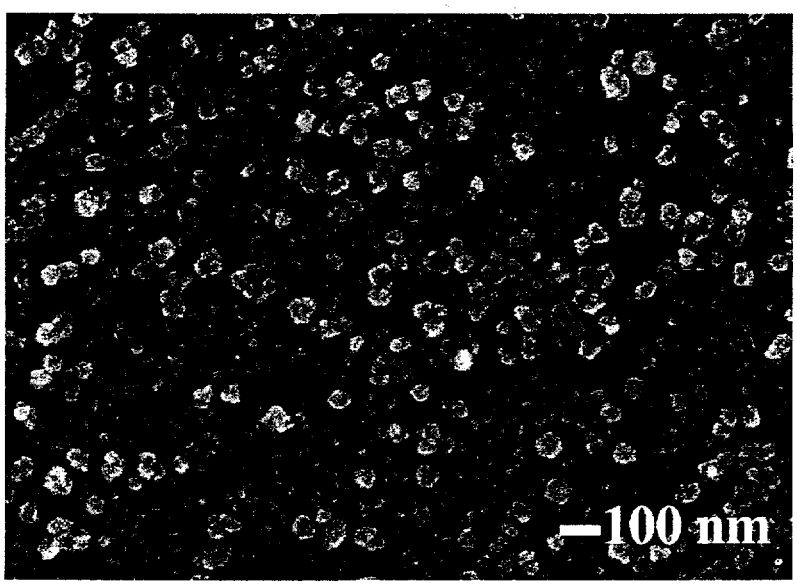

Figure 12 High resolution SEM image of the gold spheres electrodeposited onto W from $AuCl_3$. Total charge passed was approximately 30 $x10^{-3}$ Coulombs / cm^2. This particle density was found to give the optimum SERS signals.

Results and Discussion : *Effects of Hydrogen Peroxide* Potentiodynamic polarization curves for 99% W in 0.1M NaCl with and without 0.01M H_2O_2 are presented in Figure 13. This figure was generated by superimposing separate anodic and cathodic polarization curves with and without H_2O_2. The addition of H_20_2 to the chloride solution increased the OCP of the W sample, the corrosion current density of the tungsten sample, and the cathodic reaction rate (i.e. higher cathodic current densities were observed). No change in the anodic portion of the polarization curve was observed. For comparison, the anodic and cathodic polarization curves for 99.95% Ta in 0.1M NaCl and 0.1M NaCl with and without 0.01M H_2O_2 are presented in Figure 14. As before, separate anodic and cathodic curves were generated. Here, however, the anodic and cathodic plots have been separated for clarity, as shown in Figures 14a and 14b, respectively. As was the case for W in these solutions, the addition of H_2O_2 to the chloride solution increased the OCP, the corrosion current density, and the cathodic reaction rate (Figure 14b) of the Ta sample. In contrast to the W sample, however, the anodic dissolution rates of the Ta sample were nearly two orders of magnitude lower than those observed for W in the identical solution.

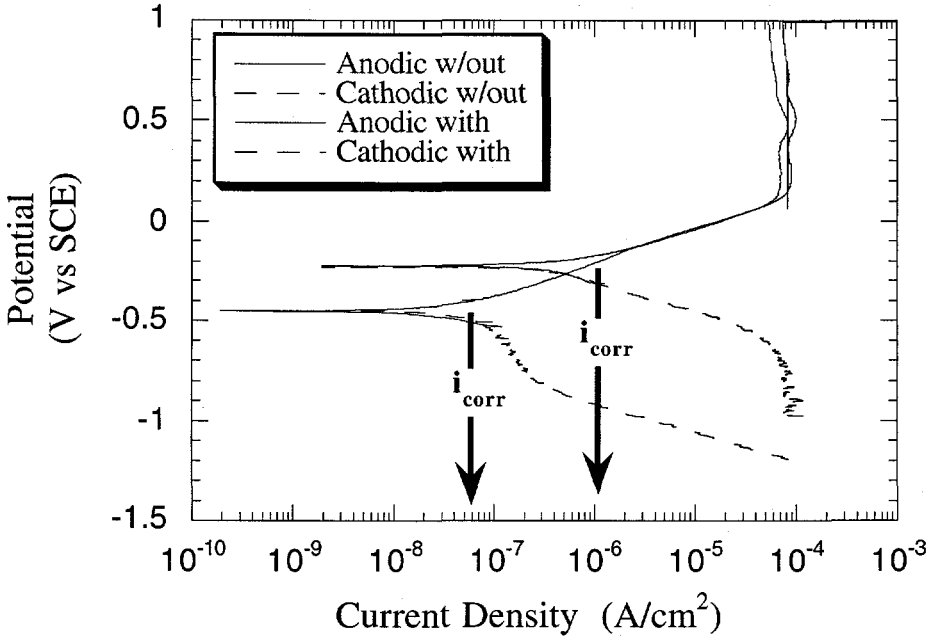

Figure 13 Anodic and cathodic potentiodynamic polarization curves for 99% tungsten in 0.1M NaCl with and without the addition of 10mM of hydrogen peroxide. Peroxide has no apparent effect on the anodic dissolution rates, however, markedly increases the cathodic reaction rate (increased cathodic currents and OCP).

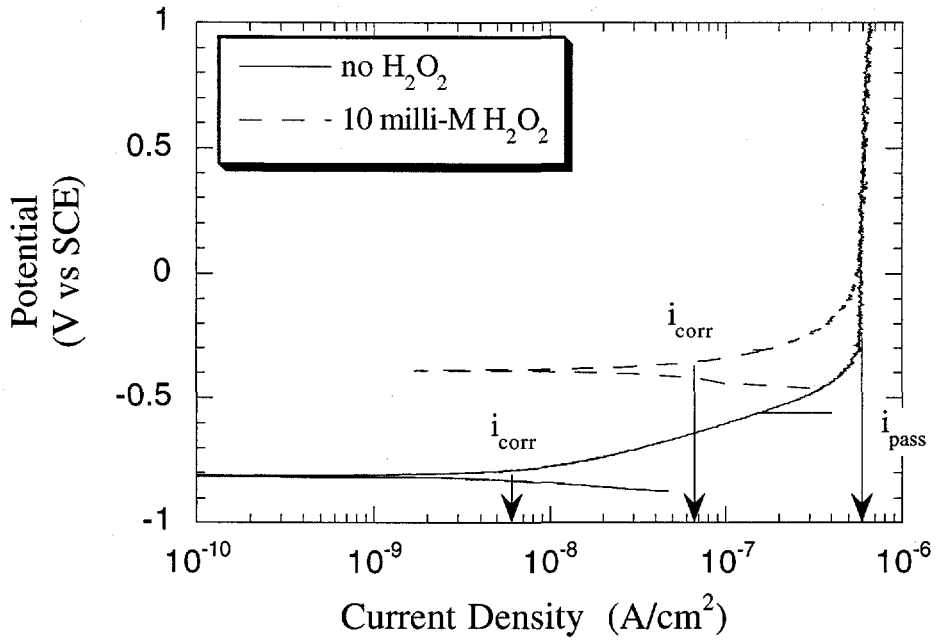

Figure 14a Anodic potentiodynamic polarization curves for tantalum in 0.1M NaCl with and without the addition of 10mM hydrogen peroxide. Peroxide increase the OCP, however, no effect on anodic reaction kinetics were observed.

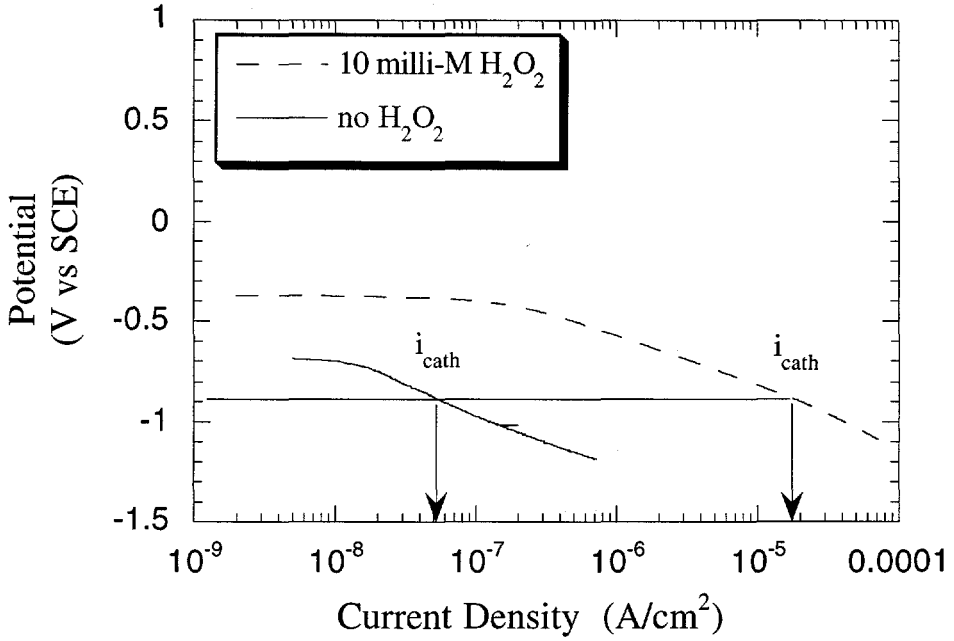

Figure 14b cathodic potentiodynamic polarization curves for tantalum in 0.1M NaCl with and without the addition of 10mM hydrogen peroxide. Hydrogen peroxide increases the cathodic reaction rate (cathodic current, i_{cath}) for an equivalent driving force (i.e., equal applied potentials).

Collectively these results indicate that the only effect of hydrogen peroxide on W or Ta is to increase the cathodic reaction kinetics. This increase may be due either to direct electrochemical decomposition of peroxide:

$$H_2O_2 + 2H^+ + 2e^- \leftrightarrow 2H_2O \qquad \text{Eq. 5}$$

or due to the formation of oxygen during the chemical decomposition:

$$\begin{array}{rl} H_2O_2 + 2H^+ + 2e^- \leftrightarrow 2H_2O & \\ \underline{H_2O_2 \qquad\qquad \leftrightarrow O_2 + 2H^+ + 2e^-} & \\ 2H_2O_2 \qquad\qquad \leftrightarrow 2H_2O + O_2 & \end{array} \qquad \text{Eq. 6}$$

which also increases the cathodic reaction rate:

$$O_2 + 4H^+ + 4e^- \leftrightarrow 2H_2O \qquad \text{Eq. 7}$$

Because corrosion reactions are generally cathodically limited, the effect of an increased cathodic reaction rate (i.e. higher cathodic current densities) is the observed increase in OCP and corrosion current density. It is important to note that while it may be theoretically possible for hydrogen peroxide to directly oxidize W(IV) in the film (or the mixed oxide W_2O_5) to W(VI) according to the reaction sequence:

$$\begin{array}{ll} H_2O_2 + 2H^+ + 2e^- & \leftrightarrow 2H_2O \\ W(IV)_{oxide} & \leftrightarrow W(VI)_{oxide} + 2e^- \\ \hline H_2O_2 + 2H^+ + W(IV)_{oxide} & \leftrightarrow 2H_2O + W(VI)_{oxide} \end{array} \qquad \text{Eq. 8}$$

It should be noted that the open circuit potential of W was more positive than the W(VI) oxidation potential of -0.683V SCE at pH 7. As further evidence that Eq. 8 does not play a role in the corrosion mechanism for W, hydrogen peroxide did not affect the W anodic reaction rates as shown in Figure 13. This may be because both WO_2 (or the mixed oxide) and WO_3 are equally stable and no net effect of oxidation from the (IV) to the (VI) state was observed in the polarization curves. The conclusion is that hydrogen peroxide does not affect the passivity of tungsten (or Ta) as observed above (Figures 13 and 14). It has been suggested that hydrogen peroxide is responsible for the oxidation of the mixed oxide W_2O_5 to the soluble species WO_5^{-2} in 9.8M H_2O_2[**36,37**]. However, 9.8M H_20_2 / 0.2M K_2SO_4 is slightly acidic, pH=4-5, and as indicated by the Pourbaix diagram this oxidation reaction is not possible without a change in the solution pH to more alkaline values. Further, metal hydrolysis would only serve to decrease the pH of this solution.

Effect of Solution pH and Material Purity Potentiodynamic polarization curves for 99.95% W in deaerated solution as a function of pH are presented in Figure 15. No pitting potentials for W were observed at any pH in the measured potential range. As indicated by the low current densities and shape of the pH 7 polarization curve, W appears to be passive at this pH. This is also indicated by the negative histeresis in the reverse scan of the W pH 7 data. At lower pH, higher anodic current densities were noted and no negative histeresis in the reverse scan was observed.

The highest anodic dissolution rates were observed in alkaline solutions. While the pH 10 dissolution rates are in agreement with the thermodynamic data[**38**], the relative dissolution

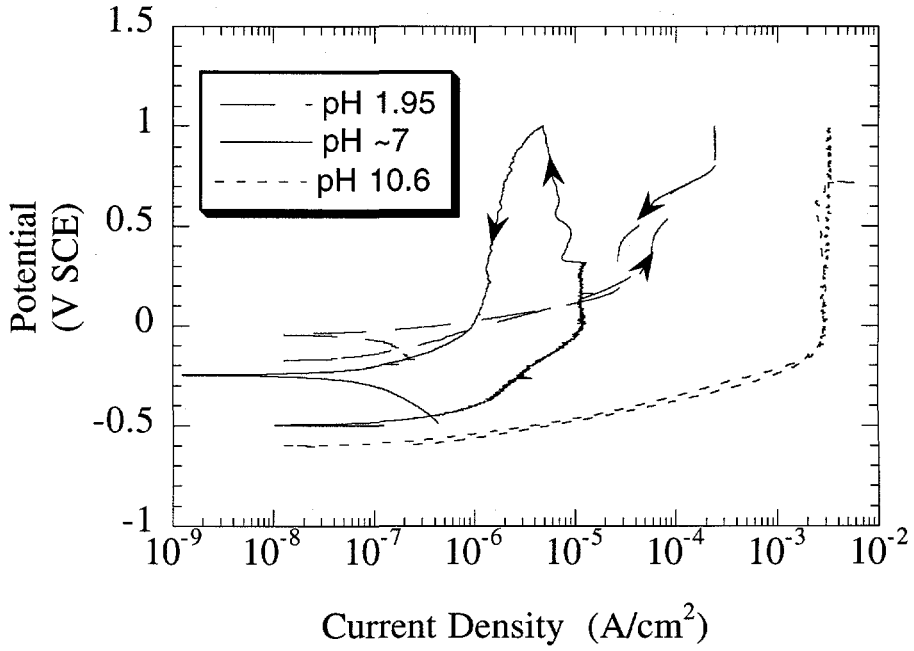

Figure 15 Potentiodynamic polarization curves for 99.95% W target material in deaerated 0.10M NaCl as a function of solution pH. Forward and reverse scans are shown.

rates of the pH 7 and pH 2 data do not appear to agree with the thermodynamic stability of tungsten oxide. From the thermodynamic data one might predict that in slightly to strongly acidic solutions W is passive as the W-oxides (WO_2, W_2O_5 and, WO_3) are thermodynamically stable in this pH range. In near neutral to alkaline solutions the divalent tungstic anion is thermodynamically favorable. One might conclude that the dissolution rates in pH 2 solution would, therefore, be lower than those at pH 7. This would be true because all potentials at a solution pH of 2 are more positive than the W oxide formation potential (Figure 16) and further to the left of the WO_3/WO_4^{-2} oxidation line. However, this is not observed in the polarization behavior, i.e. the dissolution rates are higher in solutions more acidic than pH 7. The thermodynamic relationships used to calculate Figure 16 do not account for kinetic behavior which may explain the apparent discrepancy between the equilibria diagram and the potentiodynamic polarization data.

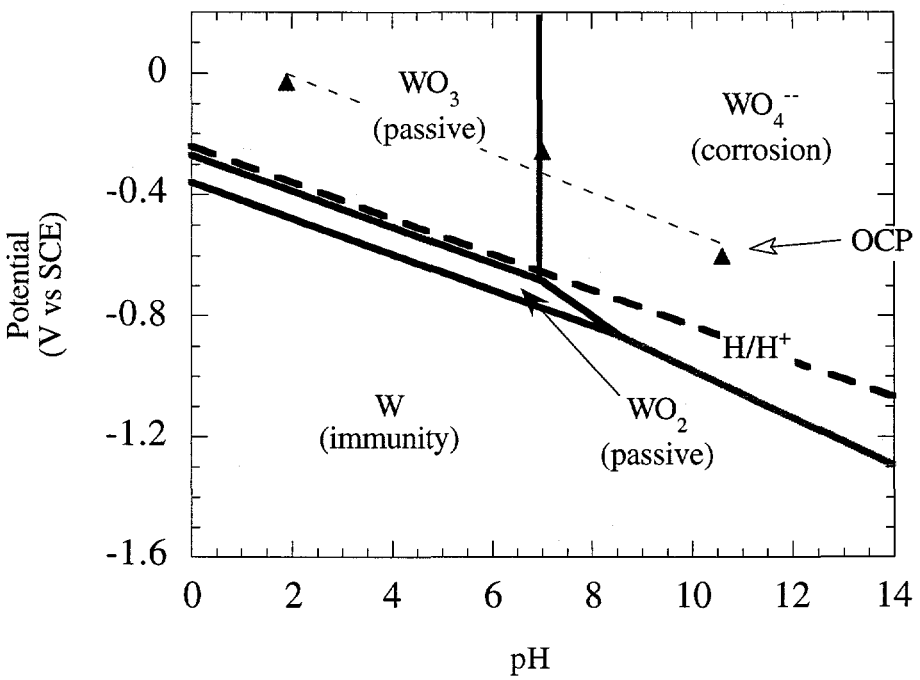

Figure 16 Electrochemical equilibria diagram for W in water. Diagram depicts areas of immunity, passivity, and corrosion as well as the respective thermodynamically stable species in that region. W_2O_5 line was removed for clarity. Calculations assume 1M dissolved species where applicable.

For comparison, the polarization curves for machinable tungsten as a function of solution pH are presented in Figure 17. For clarity only the forward scan direction is presented. Unlike the 99.96% W sample, no passivity was observed for this sample at any solution pH. All curves were characterized by high dissolution rates (greater than 10^{-5} A/cm^2) and no hysteresis in the reverse scan. Furthermore, two anodic peaks at approximately +0.2V and +0.7V SCE not observed in the 99.95% sample were observed in the forward anodic scan for this sample. Upon removal from the pH 10.6 solutions, the machinable tungsten was coated with a thick (0.5 mm), aqua-green oxide (Figure 18). After several hours of exposure to air the color of this oxide turned from aqua green to white. In addition, and copious amounts of white precipitate were found in the electrochemical cell used for the pH 10.6 experiment. X-ray photoelectron spectroscopy found the oxide to be copper-rich. At this time it is unclear if these peaks in the forward anodic scan are associated with

the oxidation of copper as no reduction peaks were found upon reversing the scan direction (see Figure 18).

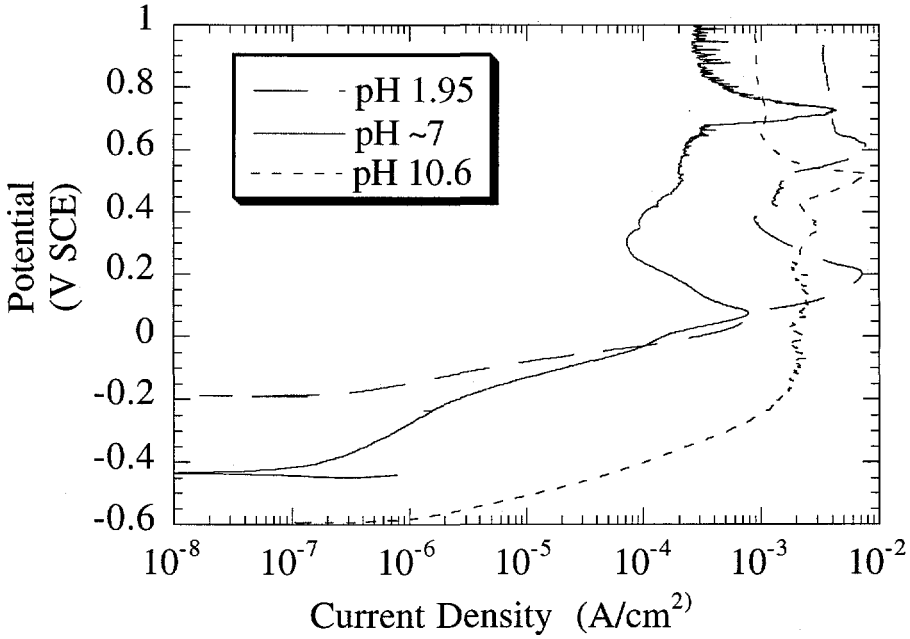

Figure 17 Potentiodynamic polarization curves for machinable tungsten in deaerated 0.1M NaCl solution as a function of solution pH. Only forward scans are shown for clarity. Anodic peak at approximately +0.20V was also observed in reverse scan.

Figure 18 Optical micrograph of machinable tungsten sample after anodic polarization in 0.1M NaCl, pH 10.6. The copper-rich oxide was as thick as 0.5mm in some places.

Anodic potentiodynamic polarization curves for 99.96% W, machinable W, and 99% W in 0.1M NaCl pH 7 are presented in Figure 19. Both forward and reverse scan directions are shown. All samples had approximately the same OCP (-0.50V to -0.40V SCE). The corrosion current density of the machinable W sample was highest ($8x10^{-8}$ A/cm^2) while that of the 99% W was lowest ($2x10^{-8}$ A/cm^2). However, the anodic behavior of each sample, was vastly different. The 99.96% W had the lowest anodic dissolution rates and a negative hysteresis in the reverse scan direction indicating passivition of this sample. Anodic dissolution rates for the 99% W sample upon polarization in this same solution were an order of magnitude greater than those observed in the APT target material. No hysteresis was observed in the reverse scan indicating the dissolution may be mass transport limited and the oxide film formed on this sample was not passivating. The anodic dissolution rates for machinable tungsten in this solution were two orders of magnitude greater than those observed for the 99.96% pure W target material and peak anodic currents were

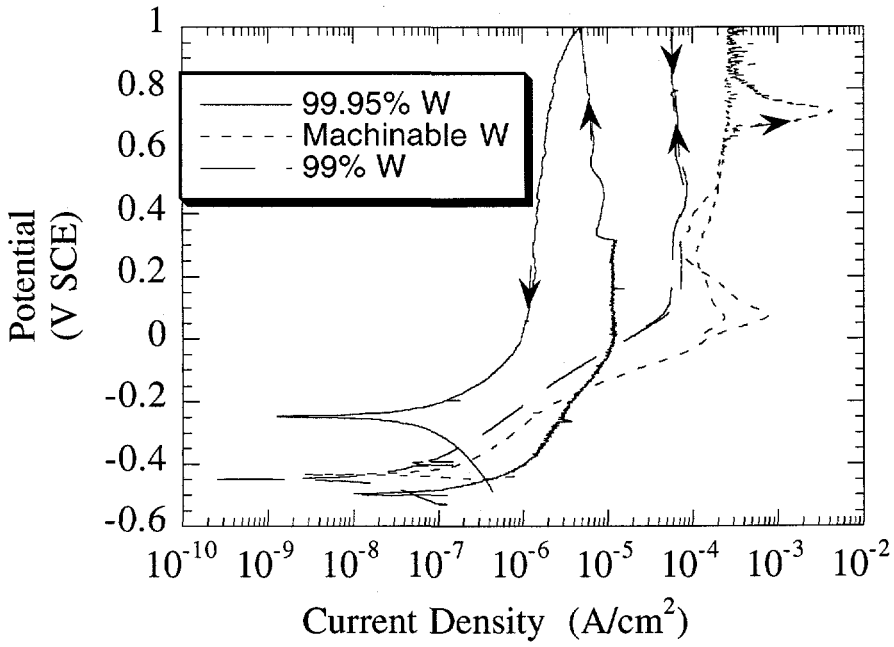

Figure 19 Potentiodynamic polarization curves for 99.95% W, machinable W and, 99% W in deaerated 0.1M NaCl, pH 7. Forward and reverse scan directions are shown.

greater than $1x10^{-3}$ A/cm^2. An anodic dissolution rate of $1x10^{-3}$ A/cm^2 for W (W to W^{+6}) is equivalent to a corrosion rate of approximately 200 mils/year.

Although the OCP of the W target in the cooling water loop during irradiation by a 1200 MeV proton beam will likely never be known, it is conceivable that it may coincide with one of the anodic peaks observed in the polarization curve of the machinable tungsten (-0.50V to -0.40V SCE). This is true because the presence of oxygen in the system or hydrogen peroxide will shift the OCP in a positive direction as shown above in Figure 13. Therefore, from these results it is concluded that machinable tungsten does not appear to be an acceptable target material for APT.

In Situ Characterization of the Oxide on W (SERS) Surface Enhanced Raman Spectroscopy (SERS) will be used to characterize the effects of irradiation on the oxide formed on W. For comparison, baseline SERS data on W oxide is needed as a function of solution pH and applied potential. The SERS data for the native oxide formed on W in air are presented in Figure 20 line a. As presented in Table 1, this peak position of approximately 912 cm^{-1} is consistent with the Raman spectra of bulk hydrated tungsten oxide as observed by other investigators. For comparison, the Raman peak positions of anhydrous, bulk W oxide are Presented in Table 2. As seen in Table 2, no peak Raman peaks for the anhydrous W oxides are observed in the 900 wave number region. The broadness of the peak in Figure 20a and absence of peaks at lower wave numbers is an indication that the native oxide formed on W is vitreous in character**[21]**.

The SERS spectrum for this same sample (Figure 20a) after 1 hour of immersion in 0.25M sodium borate / NaOH, pH 10.6 at the OCP is presented in Figure 20 line b. The Raman peak due to solution (approximately 780 cm^{-1}) has been subtracted from the data. The OCP of the sample in this solution was found to be -0.535V SCE and is in a potential / pH region where no solid oxide species is thermodynamically favorable (Figure 16). The species which is thermodynamically favorable in this potential / pH region is the soluble species WO_4^{-2}. The oxidation potential for W° to WO_4^{-2} is -1.037V SCE at this solution pH. As seen in Figure 20b, upon immersion of the sample the SERS peak observed in air is shifted to higher wave numbers (940 cm^{-1}). In addition,

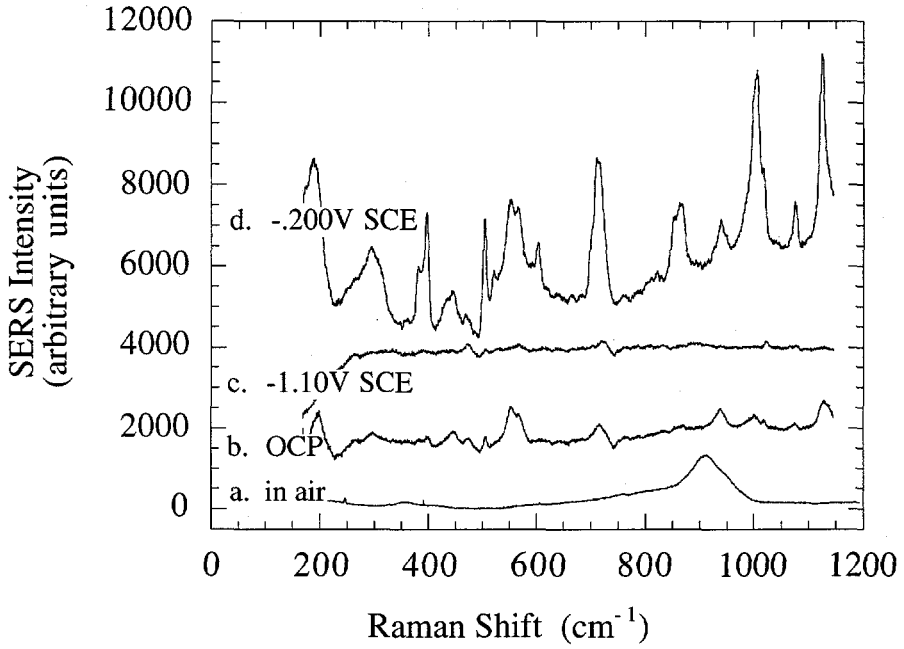

Figure 20 SERS spectra for W in 0.25M sodium borate / NaOH, pH 10.6 as a function of applied potential. The open circuit potential for W in this solution is -0.535V SCE.

several new SERS peaks not observed in air spectrum are seen in this spectrum. Their positions are listed in Table 3.

Upon polarization to -1.100V SCE, many of the SERS peaks observed at the OCP were not observed. Further, the intensities of the peaks that were observed were greatly diminished (20 line c). This is an indication that the native W oxide is reducible, though not entirely at this potential. After polarizing the sample from -1.100V SCE to -0.200V SCE (+.335V vs OCP) all of the original SERS peaks observed at the OCP (but not at -1.1V) reappeared, with greatly increase intensities (Figure 20 line d).

This data, and further SERS experiments at pH 7 and pH 2, will provide valuable background data for comparison with SERS measurements on tungsten irradiated by a proton beam in the Blue Room at LANL. Those experiments are scheduled to begin in the early November, 1996. It is hoped that any changes in the oxide film formed on W due to irradiation will be reflected in the SERS data.

Table 1 Peak positions for hydrated, bulk tungsten oxides as observed by other investigators.

Species	Wave Number (cm^{-1})									
	900	**800**	**700**	**600**	**500**	**400**	**300**	**200**	**100**	**ref**
WO_3 $2H_2O$	960			685 662			380	235 210	110	**39**
	961			650						**40**
	960			685 665						**41**
WO_3 H_2O	948			645			377	253 235	192 150	**40**
	947			650						**41**
WO_3 $1/3H_2O$	960	800		680						**42**
	955		755	670		416				**42**
	945	805		680			320	255	190 155	**40**
WO_3 xH_2O	950		770					280		**43**
	950						329		186	**44**
	950		717				329	274	186 136	**45**
Na_2WO_4	931	838					325			**45**
	931	833					324			**46**
	931	811					371 309			**47**

Table 2 Peak positions for anhydrous, bulk tungsten oxides as observed by other investigators.

Species	Wave Number (cm^{-1})									
	900	**800**	**700**	**600**	**500**	**400**	**300**	**200**	**100**	**ref**
mWO_3		807	715							**40**
hWO_3		817		690 645						**40**
misc WO_3		810	720							**48**
		808	719	625 604	580 520					**48**

Table 3 SERS peak positions measured for W immersed in 0.25M sodium borate / NaOH, pH 10.6.

Potential (V SCE)	Wave Number (cm^{-1})								
	1000	**900**	**800**	**700**	**600**	**500**	**400**	**300**	**200**
in air		912	809	756			408	360	222
-0.535 (OCP)	1073 1022	997 937	850	715		554 505	475 445 400	300	200
-1.100	1072 1024			720		566 505	472		
-0.200	1075 1021	996 936	866/85 1	715	603	566/55 1 503	472 445/43 3 400	300	198

Future Work: FY '97

Our efforts from October through January of 1996 will primarily focus on final preparations for this year's irradiation of the LANSCE A6 Corrosion Loop to begin on or about February 7, 1997. This includes assisting AOT-7 in the design of the LANSCE water system as well as preparing the many corrosion monitors for installation on this system. During this period we have also scheduled corrosion experiments for LANSCE WNR (November 16 - 18) with Gary Kanner and Luc Daemen. While their efforts will focus on on-line diagnostic techniques using Raman spectroscopy, jointly we will investigate the effect of radiation on passive films using Surface Enhanced Raman Spectroscopy (SERS) as discussed in this report.

During the FY '97 irradiation of the LANSCE A6 Corrosion Loop, numerous on-line experiments will be conducted to evaluate the corrosion rate of candidate APT materials and strategies to mitigate the effects of water radiolysis products on corrosion. These experiments will include (but are not limited to):

- In-Beam corrosion rates of: W, Ta, SS 304L, SS 316L, HT-9 and, Inconel 718
- Out-of-Beam corrosion rates of: W, Ta, SS 304L, SS 316L, HT-9 and, Inconel 718, Al 6061 and, Al 5052
- Corrosion potential measurements on out of beam specimens
- Water pH measurements
- Water conductivity measurements
- Effects of Hydrogen Water Chemistry on corrosion rates of in-beam and out of beam samples
- Water sampling to determine anion/cation concentrations of species in solution (via ICP)

Laboratory experiments on candidate APT materials will continue throughout FY '97. This will include the effects of surrogate solutions on materials in addition to tungsten. During this period we will also investigate the effects of flow and temperature on corrosion rate, two variables that APT materials will be subject to but not examined in this report.

References

1 J.L. Magee, A. Chatterjee, in Kinetics of Nonhomogeneous Processes, G.R. Freeman ed., John Wiley & Sons, New York, pp171-214, 1987.

2 H. Christensen, **Nuclear Technology**, vol. 109, pp. 373-82, 1994.

3 T.K. Yeh, D.D. Macdonald, A.T. Motta, **Nuclear Science and Enginering**, vol. 121, pp 468-82, 1995.

4 W.G. Burns, P.B. Moore, **Radiation Effects**, vol. 30, pp. 233-42, 1976.

5 R.S. Glass, G.E. Overturf, A. Van Konynenburrg, R.D. Mccright, **Corrosion Science**, vol. 26, no. 8., pp. 577-90, 1986.

6 H. Christensen, **Radiation Physical Chemistry**, vol 18, no. 1-2, pp.147-58, 1981.

7 W.G. Burns, W.R. Marsh, W.S. Walters, **Radiation Physical Chemistry**, vol. 21, no. 3, pp. 259-79, 1983.

8 M. Fox, "Water Chemistry and Corrosion in BWR's", *Corrosion/83*, paper no. 121, NACE, Houston, 1983.

9 M.E. Indig, J.E. Weber, **Corrosion**, vol. 41, no. 1, pp. 19-30, 1985.

10 J.J. Taylor, **EPRI Journal**, vol. 11, no. 3, pp. 54-55, 1986.

11 D.D. Macdonald, **Corrosion**, vol. 48, no. 3, pp.194-205, 1992.

12 D.D. Macdonald, H. Song, K. Makela, K. Yoshida, **Corrosion**, vol. 49, no. 1, pp. 8-16, 1993.

13 J.R. Macdonald, Impedance Spectroscopy, Wiley Publishing, New York, 1987.

14 I. Epelboin, C. Gabrielli, M. Keddam, H. Takenouti, "Alternating-Current Impedance Measurements and Corrosion Rate Determination", in Electrochemical Corrosion Testing, ASTM STP 727, F. Mansfeld & U. Bertocci eds., ASTM, Ohio, pg. 150-66, 1981

15 D.D. MacDonald, M.C.H. Mckubre, "Electrochemical Impedance Techniques in COrrosion Science" in Electrochemical Corrosion Testing, ASTM STP 727, F. Mansfeld & U. Bertocci eds., ASTM, Ohio, pg. 110-59, 1981

16 M. Fleischmann, P.J. Hendra, A.J. McQuillen, **Chemical Physics Letters**, vol. 26 pp 163-66, 1974.

17 J. Desilvestro, D.A. Corrigan, M.J. Weaver, **Journal of Physical Chemistry**, vol. 90, pp 6408-11, 1896.

18 A. Otto, J. Billman, J. Eickmans, U. Erturk, C. Pettenkotter, **Surface Science**, vol. 138, pp 319-27, 1984

19 M. Kerker, D.S. Wang, H. Chew, **Applied Optics**, vol. 19, pp 4159-69, 1985.

20 J. C. Rubim, J. Dunnwald, **Journal of Electroanalyitical Chemistry**, vol. 258, pp 327-344, 1989.

21 J. Gui, T.M. Devine, **Corrosion Science**, vol. 32, no. 10, pp. 1105-24, 1991.

22 C.A. Melendres, M. Pankuch, **Journal of Electroanalytical Chemistry**, vol. 333, pp. 103-13, 1992.

23 M.G.S. Ferreira, T. M. e Silva, A. Catarino, M. Pankuch, C.A. Melendres, **Journal of the Electrochemical Sociiety**, vol. 139, no. 11, pp. 3146-51, 1992.

24 L.J. Oblonsky, T.M. Devine, **Journal of the Electrochemical Society**, vol. 142, no. 11, pp. 3677-82, 1995.

25 Annual Book of ASTM Standards, 03.02, Wear and Errosion; Metallic Corrosion, ASTM Philadelphia, 1987.

26 L.B.Kriksunov, D.D. Macdonald, P.J. Millet, **Journal of the Electrochemical Society**, vol. 141, no. 11, pp. 3002-3005, 1994.

27 W.R. Kassen, "Reference Electrodes for Electrochemical Corrosion Potential Monitoring in PWR Secondary Systems", Electric Power Research Institute, EPRI TR-103311, November, 1993.

28 R.S. Lillard, D.P. Butt, "Preliminary Spallation Neutron Source Corrosion Experiments: Corrosion Rates of Engineering Materials in a Water Degrader Cooling Loop Irradiated by an 800 MeV Proton Beam", LA-UR/LA-CP 96-1011, January, 1996.

29 M.E. Indig, J.E. Weber, *Corrosion '83*, paper #124, NACE, Houston, April, 1983.

30 W.R. Kassen, R.P. Jones, J.L Tollefson, *Corrosion '92*, paper #112, NACE, Houston, April, 1992.

31 M. Fox, *Corrosion '83*, paper #121, NACE, Houston, April, 1983.

32 C.C. Lin, R.L. Cowan, R.S. Pathania, *Corrosion '93*, paper #619, NACE, Houston, April, 1993.

33 L.G. Ljungberg, D. Cubicciotti, M. Trolle, *Corrosion '85,* paper #100, NACE, Houston, March, 1985.

34 M.J. Fox, "A Review of Boiling Water Reactor Chemistry:Science Technology, and Performance", NTIS Report# NUREG/CR-5115 ANL-88-42, February, 1989.

35 Y.J. Kim,, *Corrosion '96*, paper #102, NACE, Houston, March, 1996.

36 J.E.A.M.van der Meerrakker, M. Scholten, J.J. van Oekel, **Thin Solid Films**, vol. 208, pp 237-42, 1992.

37 J.E.A.M.van der Meerrakker, M. Scholten, T.L.G.M. Thijssen, **Journal of Electroanalytical Chemistry**, vol. 333, pp 205-16, 1992.

38 M. Pourbaix, Atlas of Electrochemical Equilibria in Aqueous Solutions, NACE, Houston, 1974.

39 M.F. Daniel, B. Desbat, J.C. Lassegues, B. Gerand, M. Figlarz, **Journal of Solid State Chemistry**, vol. 67, pp. 235-47, 1987.

40 G.M. Ramans, J.V. Gabrusenoks, A.A. Veispals, **Physica Status Solidi A**, vol. 74, no. 1, pp. k41-k44, 1982.

41 I. Shiyanovskaya, T.A. Gavrilko, E.V. Gabrusennoks, **Journal of Molecular Structure**, vol. 293, pp. 295-98, 1993.

42 I. Shiyanovskaya, H. Ratajczak, J. Baran, M. Marchewka, **Journal of Molecular Structure**, vol. 348, pp.99-102, 1995.

43 M.F. Daniel, B. Desbat, J.C. Lassegues, R. Garie, **Journal of Solid State Chemistry**, vol. 73, pp. 127-139, 1988.

44 T. Nishide, K, Mizukami, **Thin Solid Films**, vol. 259, pp. 212-17, 1995.

45 N. Weinstock, H. Schulze, A. Muller, **The Journal of Chemical Physics**, vol, 59, no. 9, pp. 5063-67, 1973.

46 F. Gonzalez-Vilchez, W.P. Griffith, **Journal of the Chemical Society, Dalton Transactions**, vol. 1, pp. 81-4, 1974.

47 F.D. Hardcastle, I.E. Wachs, **Journal of Raman Spectroscopy**, vol. 26, pp. 397-405, 1995.

48 E. Salje, **Acta Crystallography**, vol. A31, pp. 360-63, 1975.

Appendix A

Schematic Diagrams of the Plumbing System for the Corrosion Insert

courtesy of AOT-7:

Robert Brown
Eugene Zimmerman

Diagram 1: Detailed Drawling of the Plumbing System which will Circulate Cooling Water Through the Corrosion Insert. Diagram Also Depicts Placement of the "Out-of Beam" Corrosion Experiments.

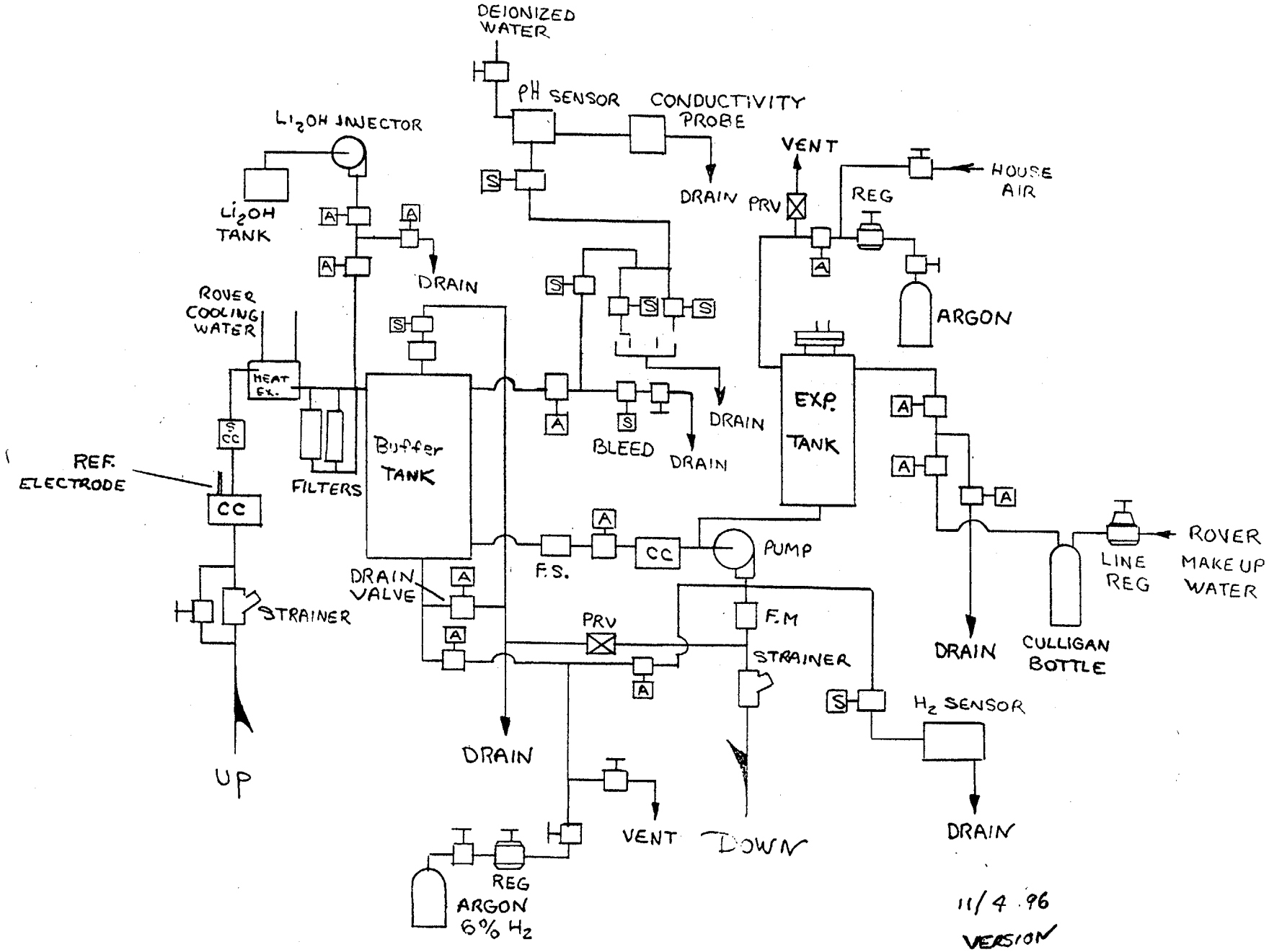
DEIONIZED WATER
pH SENSOR
CONDUCTIVITY PROBE
DRAIN
VENT
PRV
HOUSE AIR
REG
ARGON
Li_2OH INJECTOR
Li_2OH TANK
DRAIN
ROVER COOLING WATER
HEAT EX.
EXP. TANK
BLEED
DRAIN
DRAIN
REF. ELECTRODE
CC
FILTERS
Buffer TANK
F.S.
PUMP
LINE REG
ROVER MAKE UP WATER
DRAIN VALVE
STRAINER
PRV
F.M
STRAINER
DRAIN
CULLIGAN BOTTLE
H_2 SENSOR
DRAIN
UP
DRAIN
VENT
DOWN
REG
ARGON
6% H_2
11/4/96
VERSION

Appendix B

Schematic Diagrams of the Corrosion Insert

courtesy of AOT-7:

Robert Brown
Joe Vasquez

Diagram 1: In Beam Corrosion Experiments Depicting In Beam Tube Array, High Neutron Flux Stress Corrosion Cracking Sample Holder and, High Neutron Flux Tube Array

Diagram 2: Detailed Drawling of In-Beam / High Neutron Flux Corrosion Tube Array and Placement of the Corrosion Probes

Diagram 3: Detailed Drawling of the Stress Corrosion Cracking Sample Holder and Placement of Stress Corrosion Cracking Samples

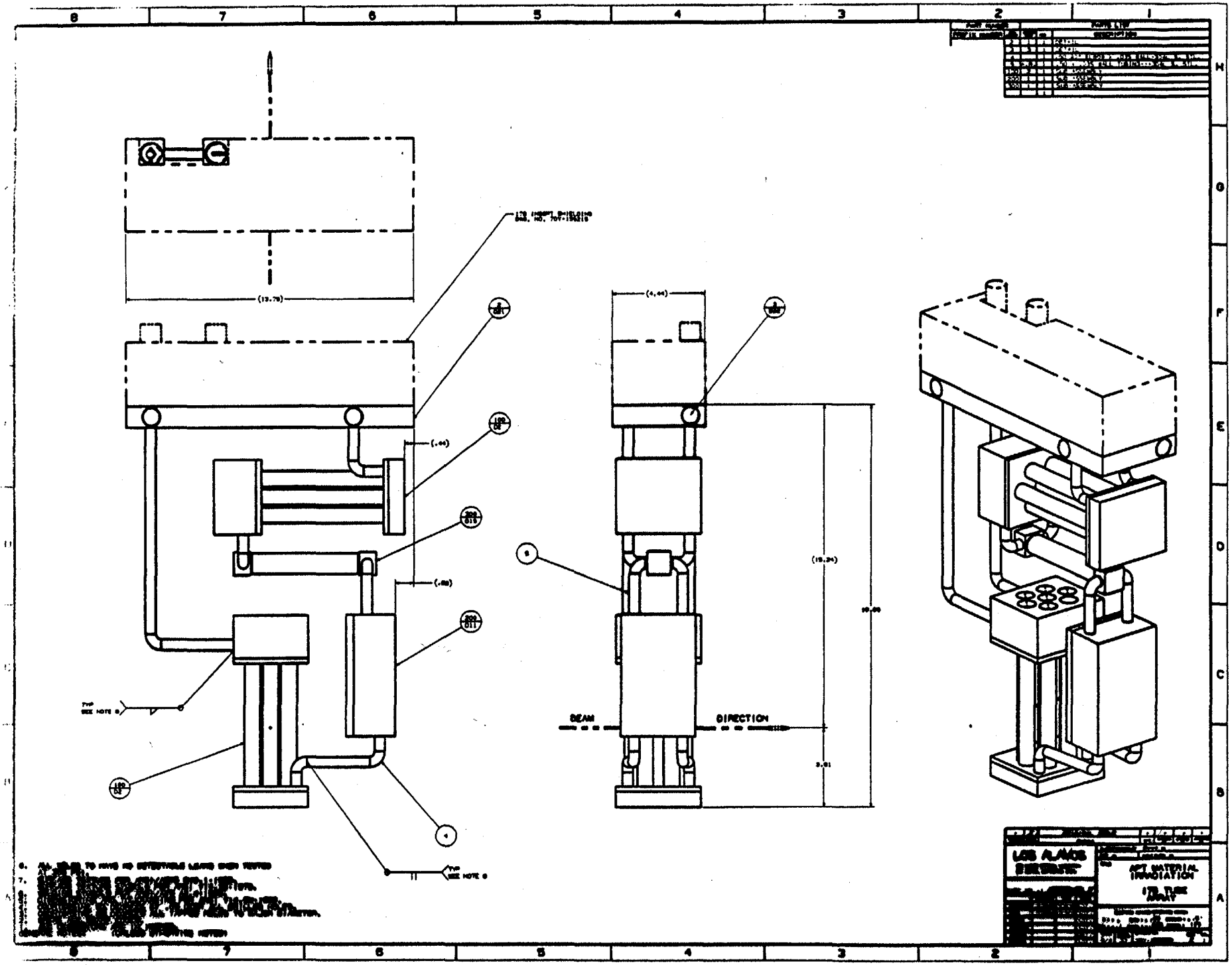
BEAM
DIRECTION

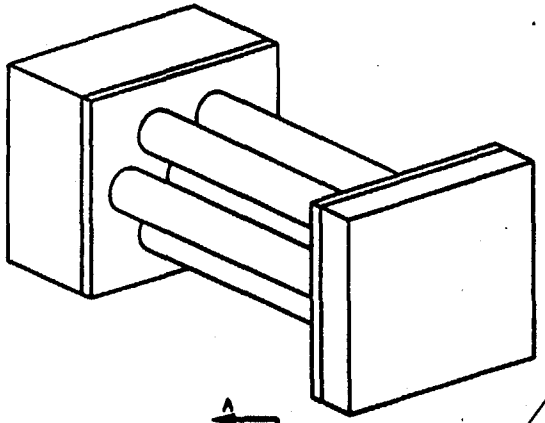

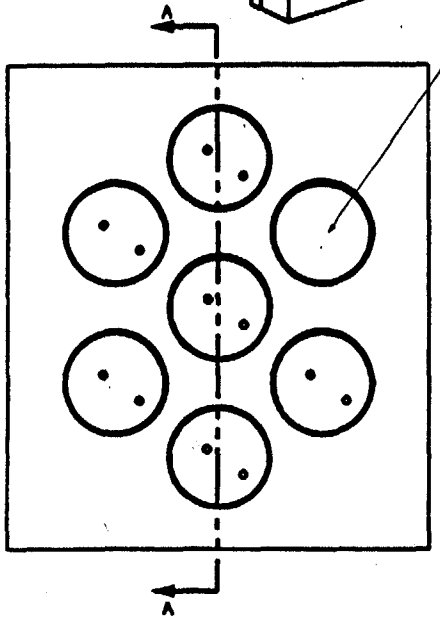

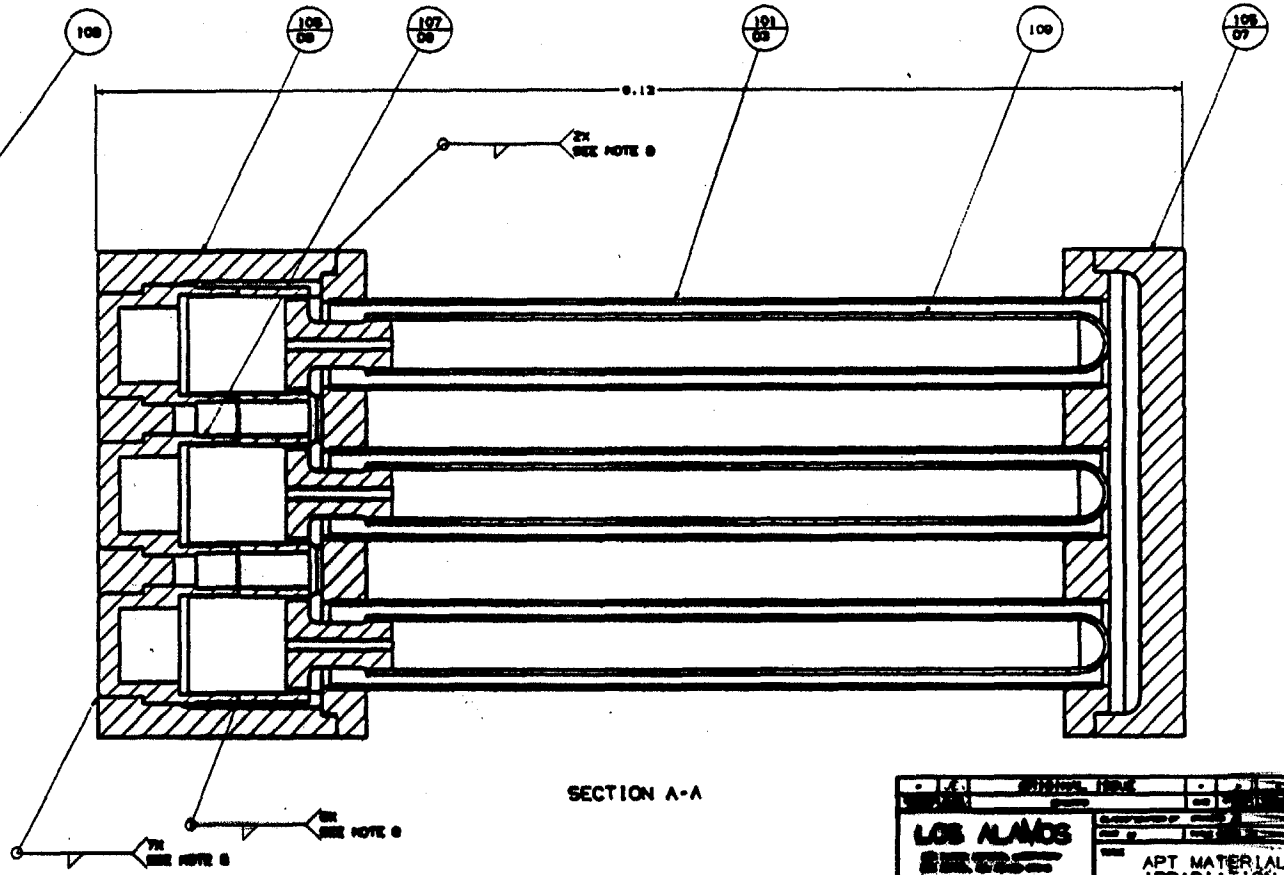

SECTION A-A

PART NUMBER			PARTS LIST	
PREFIX NUMBER	QTY	MAT'L		DESCRIPTION
101	1	103	DETAIL	
105	1	120	DETAIL	
106	1	100	DETAIL	
107	6	100	DETAIL	
108	1	100	DETAIL	
109	6	100	KOVAR & STAINLESS STEEL PROBES---- TO BE FURNISHED BY USER	

8. ALL WELDS TO HAVE NO DETECTABLE LEAKS WHEN TESTED AT 300 PSI.
7. [illegible]
GENERAL NOTES: (UNLESS OTHERWISE NOTED)

LOS ALAMOS

APT MATERIAL IRRADIATION

17B TUBE ARRAY

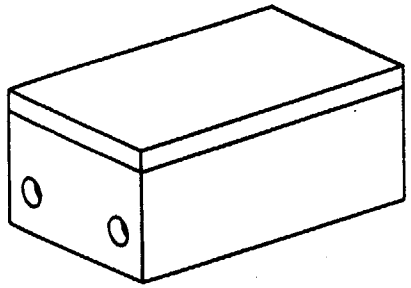

PART NUMBER		PARTS LIST	
PREFIX NUMBER	ITEM	QTY	DESCRIPTION
-200	201	1	DETAIL
	202	1	DETAIL
	203	1	DETAIL
	204	24	CORROSION SAMPLES - FURNISHED BY USER
	205	12	CORROSION SAMPLES - FURNISHED BY USER

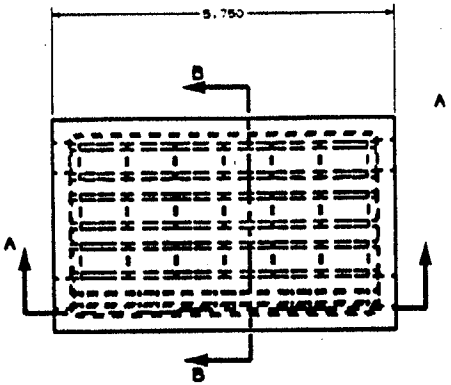

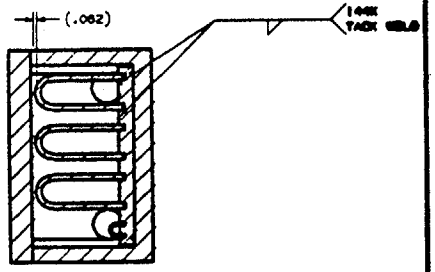

SECTION B-B

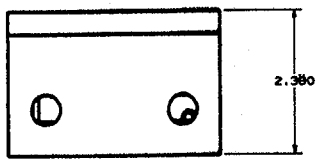

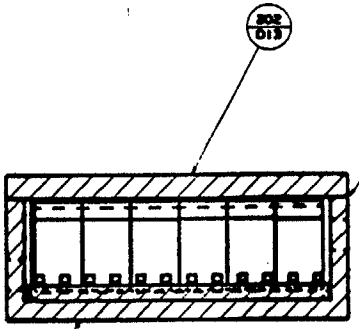

SECTION A-A

8. ALL WELDS TO HAVE NO DETECTABLE LEAKS WHEN TESTED AT 300 PSI.
7. SURFACE TEXTURE PER ANSI/ASME B46.1-1985.
SURFACE TEXTURE SYMBOLS PER ANSI Y14.36-1978.
6. WELDING SYMBOLS PER ANSI/AWS A2.4-1986.
5. DIMENSIONING AND TOLERANCING PER ANSI Y14.5-1982.
4. COUNTERSINK AS DETAILED BY .03 DEEP ALL DRILLED HOLES.
3. COUNTERSINK AS DETAILED ALL TAPPED HOLES TO MAJOR DIAMETER.
2. BREAK ALL SHARP EDGES.
1. ALL DIMENSIONS ARE IN INCHES.
GENERAL NOTES: (UNLESS OTHERWISE NOTED)

300

LOS ALAMOS

PART NO. -200

APT MATERIAL IRRADIATION

178 TUBE ARRAY

76Y-198230 D 11